VOL. 11 No. 11, pp. 313-340 MAY 1950

Philips Technical Review

DEALING WITH TECHNICAL PROBLEMS
RELATING TO THE PRODUCTS, PROCESSES AND INVESTIGATIONS OF
THE PHILIPS INDUSTRIES

EDITED BY THE RESEARCH LABORATORY OF N.V. PHILIPS' GLOEILAMPENFABRIEKEN, EINDHOVEN, NETHERLANDS

GYROMAGNETIC PHENOMENA OCCURRING WITH FERRITES

by H. G. BELJERS and J. L. SNOEK. 538.245:538.69:621.3.017.39

Non-metallic magnetic materials (ferrites marketed by Philips under the trade name "Ferroxcube") have recently attracted attention on account of their favourable properties, such as low eddy-current losses, hysteresis losses and after-effect losses. The upper limit of the useful frequency range, from the point of view of losses, varies between 10^5 and 10^8 c/s according to the material. When this limit is exceeded losses arise which increase rapidly with the frequency. It is probable that these additional losses are to be ascribed to gyromagnetic phenomena inherent in all magnetic materials. The theoretical and practical significance of these phenomena is explained.

When a ferromagnetic material is placed inside a coil carrying a constant current, then, as is known, the magnetic flux through the coil is increased. Upon the coil being connected to a source of alternating current the inductance is found to have increased. As a rule, however, even when the resistance of the coil may be ignored, the alternating voltage across the coil is no longer exactly in quadrature with the alternating current, owing to the losses occurring in the material.

These losses may in the first place be due to eddy currents in the ferromagnetic material, in which case one speaks of eddy current losses. These increase with the frequency and depend not only upon the properties of the material (conductivity and permeability) but also upon its dimensions [1]).

By making a suitable choice of the dimensions (lamination) and of the properties of the material the eddy current losses can often be made negligible, but still other losses remain which, apart from the frequency, depend only upon the properties of the material and not upon the dimensions. First of all there are the hysteresis losses, which are connected with the fact that the induction B, plotted as a function of the field strength H, shows what is called a hysteresis loop. The hysteresis losses per cycle and per unit of volume of the material are equal to the area of the hysteresis loop.

[1]) See, e.g., J. L. Snoek, Philips Techn. Rev. 2, 77-83, 1937.

In the second place there are the magnetic after-effect losses. These losses have been dealt with at length in an article by Snoek and Du Pré [2]). They are usually small and are presumably to be regarded as connected with the gyromagnetic losses dealt with in the present article.

Let the magnetic alternating field in the material be $H = H_m \cos \omega t$. Owing to after-effect and hysteresis [3]) the induction B will be shifted in phase with respect to H, so that we may write $B = B_m \cos(\omega t - \delta)$. Applying the usual complex method of expression, these formulae become:

$$H = H_m e^{j\omega t} \quad \text{and} \quad B = B_m e^{j(\omega t - \delta)} \quad . \quad . \quad (2)$$

Thus the permeability μ, which equals the quotient B/H, is complex, and naturally the relative permeability μ_r is likewise complex ($\mu_r = \mu/\mu_0$, where $\mu_0 = 4\pi \times 10^{-7}$ H/m). Thus for μ_r we have the formula

$$\mu_r = \frac{B}{\mu_0 H} = \frac{B_m e^{-j\delta}}{\mu_0 H_m} = \frac{B_m}{\mu_0 H_m} (\cos \delta - j \sin \delta).$$

Denoting $(B_m/\mu_0 H_m) \cos \delta$ by μ_r' and $(B_m/\mu_0 H_m)$

[2]) J. L. Snoek and F. K. Du Pré, Several after-effect phenomena and related losses in alternating fields, Philips Techn. Rev. 8, 57-64, 1946.

[3]) In the case of hysteresis the induction is not purely sinusoidal as a function of time; higher harmonics also occur. As regards the losses, however, we have only to do with the fundamental oscillation, and this shows a phase shift with respect to H.

sin δ by μ_r'' we can write for the complex (relative) permeability:

$$\mu_r = \mu_r' - j\mu_r'' \quad \ldots\ldots\ldots \quad (3)$$

The absolute value $|\mu_r|$ is $\sqrt{\mu_r'^2 + \mu_r''^2}$; when δ is a small angle then $|\mu_r| \approx \mu_r'$. Further, for the loss angle δ we have the formula $\tan\delta = \mu_r''/\mu_r'$.

Attention has recently been drawn to a certain kind of non-metallic magnetic materials, namely the ferrites, marketed by Philips under the trade name "Ferroxcube". These materials have a low conductivity ($\sigma = 10^{-3}$ to 10^{-5} Mho/m (= ohm^{-1} m^{-1})), and consequently the eddy-current losses are negligibly small, whilst also the hysteresis losses are generally relatively small. In a large frequency range (upper limit 10^5—10^8 c/sec, according to the material) the values of the quantity $\tan\delta$ are therefore quite small (e.g. 0.01). The losses occurring in this frequency range are to be ascribed to after-effect. However, in contrast to other cases where this has been thoroughly investigated (see footnote [2]), little is as yet known with certainty regarding the nature of this after-effect in ferrites. When the limit just mentioned is exceeded, in the case of ferrites there is a considerable increase in the value of μ_r'', accompanied by a decrease of μ_r', as is to be seen from *fig. 1* where the quantities μ_r' and μ_r'' have been plotted for a number of kinds

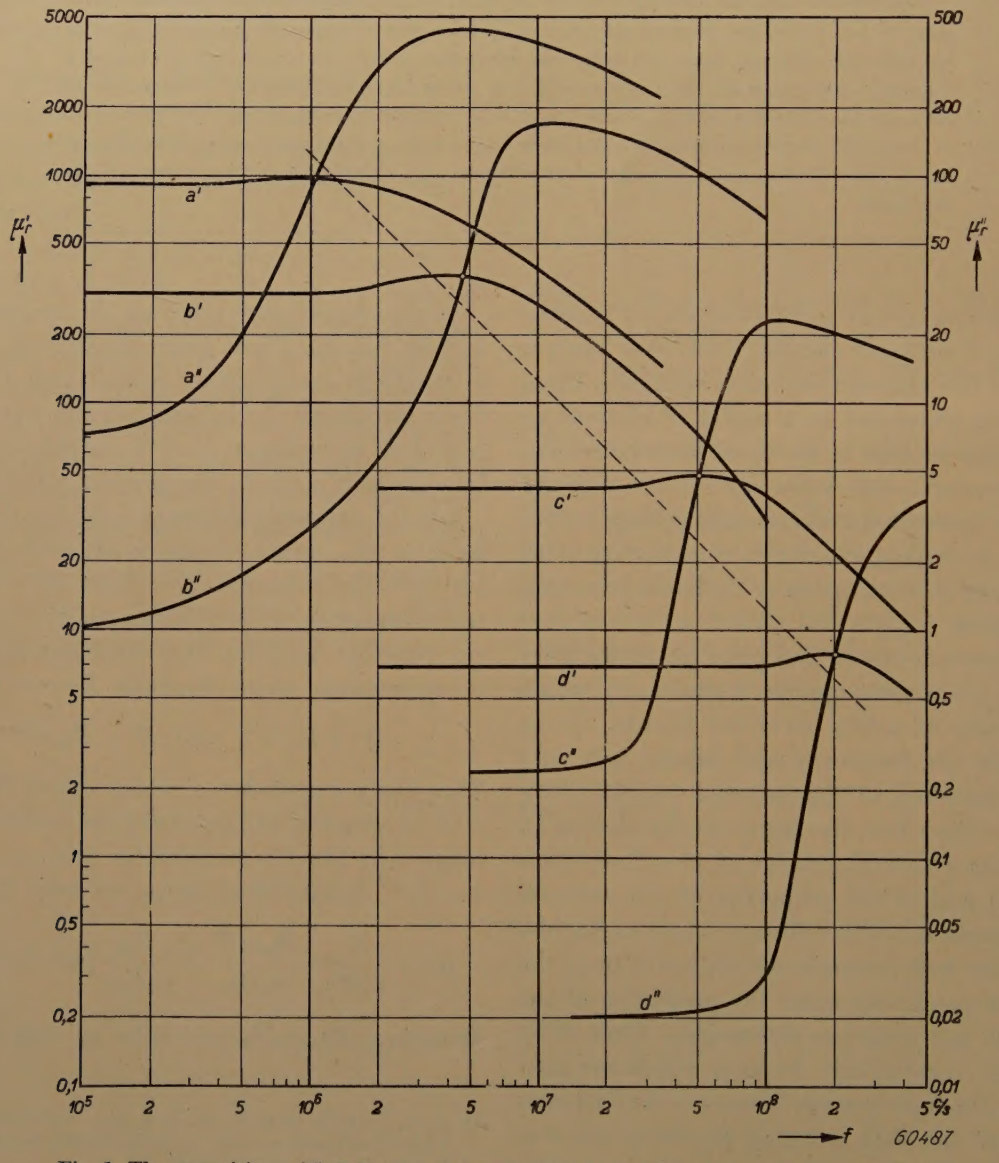

Fig. 1. The quantities μ_r' (left-hand scale) and μ_r'' (right-hand scale) for a manganese-zinc ferrite (*a*) and for a number of nickel-zinc ferrites of different composition (*b-d*). The small circles denote the points where $\tan\delta = 0.1$. The dotted line indicates the mean relation between the value of μ_r' (in the low-frequency range) of a certain ferrite and the critical frequency setting a limit to the range within which that ferrite can be used in filter coils ($\tan\delta = 0.06$).

of "Ferroxcube" as functions of frequency on a logarithmic scale [4]).

In the case of filter coils the critical frequency is generally assumed to be that at which tan δ reaches the value 0.06. From fig. 1 it appears that this critical frequency increases according as μ_r' in the low-frequency range is smaller. For application in transformers the material can be used at much higher frequencies.

The sharp increase of tan δ at high frequencies depends upon various factors. For instance, if the material shows internal stresses the increase of tan δ begins at lower frequencies than is the case with the same material free of internal stresses. After annealing, the high values of tan δ have shifted to higher frequencies. When a new material is prepared by sintering together a mixture of different ferrites it is often found that the large losses appear at lower frequencies, this being particularly the case if the ferrites have not been intimately mixed prior to the sintering; more thorough mixing shifts the region of high losses to higher frequencies.

It appears that the cause of the additional losses found in ferrites at very high frequencies is to be sought in a phenomenon theoretically predicted by Landau and Lifshitz in 1935, when no practical examples of it were known to those authors. They called this phenomenon gyromagnetic resonance [5]). The nature of this gyromagnetic resonance, as subsequently found in various magnetic materials, can be explained with the aid of a simple mechanical model.

A model illustrating gyromagnetic resonance

According to the modern theory of matter, magnetism is ascribed mainly to the fact that an electron may be regarded as a charged sphere rotating about an axis and thus showing a magnetic moment, or "spin". In a magnetic field this spin tends to follow the direction of the field and endeavours to take up a position where the potential energy is a minimum, just as is the case, for instance, with a pendulum in a gravitational field.

In addition to being charged, however, the electron also has mass, and as a result of its behaving like something that rotates it is not only a carrier of a magnetic moment but also a carrier of a mechanical angular momentum.

[4]) The data of fig. 1 are taken from unpublished measurements by C. M. van den Burgt and M. Gevers. See also J. L. Snoek, Philips Techn. Rev. **8**, 353-360, 1946.

[5]) L. Landau and E. Lifshitz, Phys. Z. Soviet Union **8**, 153-169, 1935. J. H. E. Griffiths, Nature **158**, 670, 1946. C. Kittel, Phys. Rev. **71**, 270-271, 1947. See also D. Polder, Physica The Hague **15**, 253-255. 1949 (Nos 1/2) and Phil. Mag. London **40**, 99-115, 1949 (No. 1).

The picture of the pendulum, therefore, has to be completed by imagining a spinning-top to be contained in the body of the pendulum with its axis of rotation directed towards the point of suspension. Such a pendulum is schematically represented in *fig. 2a*. This "spinning-top pendulum" behaves

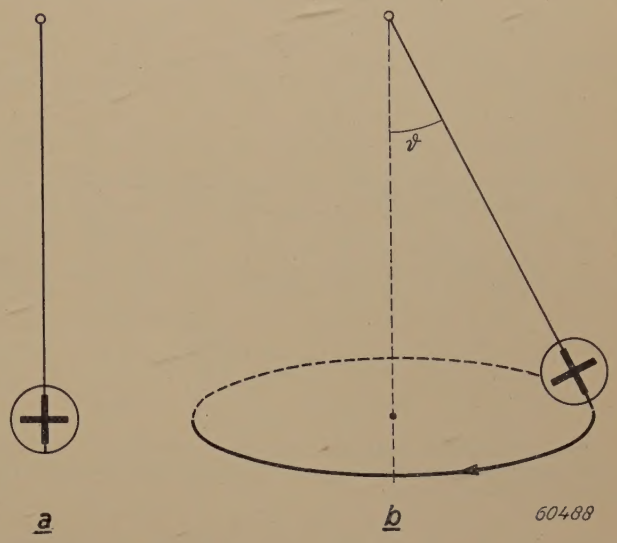

Fig. 2. Spinning-top pendulum (*a*) in the position of minimum potential energy and (*b*) making a precessional movement at an angle ϑ with the vertical.

quite differently from an ordinary pendulum, in that when the pendulum arm is moved an angle ϑ away from the vertical and then released, the pendulum does not begin to oscillate in the normal way in a plane determined by the starting position and the vertical through the point of suspension. Instead of that, the released pendulum arm begins to describe the surface of a cone with ϑ as half the apex angle (fig. 2*b*), each point along the arm thereby describing a horizontal circle. The spinning-top pendulum is then said to make a precessional movement.

The angular frequency (= angular velocity) of this precession is

$$\omega_p = M/J\,, \quad \ldots\ldots\ldots \quad (4)$$

where $M = Gl$ (G = weight of the pendulum, l = distance from the centre of gravity to the point of suspension; the couple driving the pendulum towards the position of equilibrium is therefore $Gl \sin \vartheta = M \sin \vartheta$). Further, $J = I_r\omega_r$ and is the angular momentum of the top spinning around its axis (I_r = moment of inertia about the axis of rotation, ω_r = the angular velocity of that rotation). It is seen that the angular velocity ω_p is independent of the angle of deflection ϑ.

Obviously what has been stated above no longer holds when ω_r, and thus J, is made to approach zero, since in that case the top comes to a standstill and the spinning top pendulum is no longer to be distinguished from an ordinary pendulum. The manner in which the movement of the released pendulum changes into the precessional movement as the value of J increases is to be seen from *fig. 3*, where *a* represents the

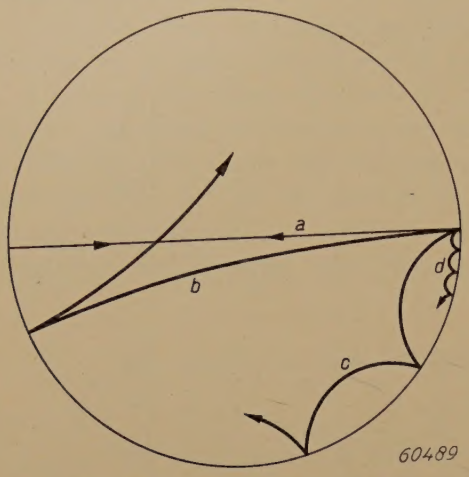

Fig. 3. Transition from the normal pendulum movement to the precessional movement as the speed of rotation ω_r of the spinning top increases.

movement (seen from above) of a point along the pendulum arm when $J = 0$. If the value of J is small then a figure will be described as indicated by *b*. As J increases *b* changes into *c*, until eventually a sort of cycloid like that at *d* is described which ultimately becomes the precessional movement along the circle.

From what has been said it will be evident that the precessional movement of the spinning-top pendulum must not be confused with the movement made by a so-called "conical pendulum"; in fact this has an entirely different frequency, viz. the same as that of an ordinary pendulum (case *a* in fig. 3).

In the transition from *a* to *d*, not only the quantity J but also the mass of the pendulum itself plays a part. But since the mass of the electron as such is of no influence it is assumed that, with our model, the above-mentioned limit has been reached.

Let us suppose that the top is rotating with its axis vertical, thus in the lowest position (as in fig. 2*a*), and that we then suddenly turn the direction of the force of gravity over a small angle ε in the plane of the drawing (*fig. 4*). It is clear that at that moment a precessional movement will begin with ε as half the apex angle and 0 and $+ 2\varepsilon$ as the extreme positions. When, after half a cycle has been completed, we suddenly cause the force of gravity to make an angle $-\varepsilon$ with the vertical, the half apex angle becomes 3ε and the extreme positions $+2\varepsilon$ and -4ε. Upon the force of gravity being caused to return to the first position ($+\varepsilon$) after another half cycle, the half apex angle becomes 5ε. Continuing in this way, at the n^{th} half cycle the apex angle becomes $(2n-1)\varepsilon$.

Thus we see that, when the force of gravity is caused to oscillate in the manner described at a rate determined by the precession, a uniform increase of the precession takes place which is to be compared to a "resonance", especially when the deflection in the plane of the interference is considered. In the case we have just been dealing with, where no account has been taken of a possible damping, the deflection may ultimately become very great, however small ε may be. As will be explained below for the case of a sinusoidal interference, for oscillations of the force of gravity at a frequency differing from ω_p one always finds a finite deflection.

Gyromagnetic resonance of electrons

The mental experiment that we have just made is not easy to carry out mechanically because we cannot govern the force of gravity, but in the magnetic case, with the means that are now at our disposal, it is fairly easy to perform.

Imagine that we have a free-spinning electron, the angular momentum of which is

$$J = \tfrac{1}{2}\,(h/2\pi)\,,$$

where h represents Planck's constant ($h = 6.6 \times 10^{-34}$ kg·m²/s). This is accompanied by a magnetic moment (Bohr magneton)

$$\mu_B = \frac{e}{m_0} J = \frac{eh}{4\pi m_0} \quad \ldots\ldots \quad (5)$$

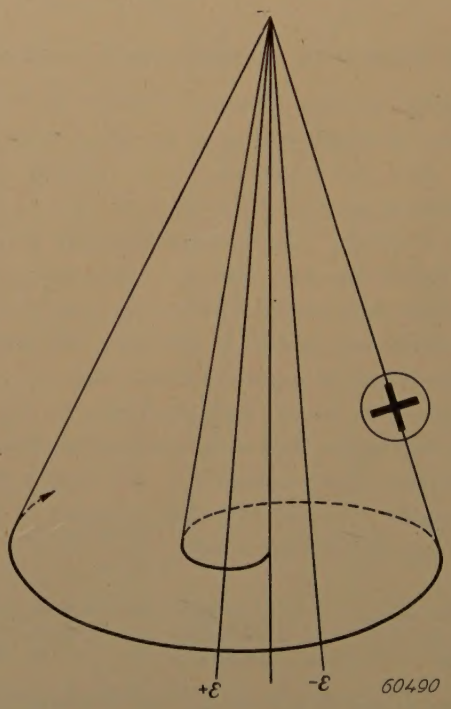

Fig. 4. Behaviour of the spinning-top pendulum when the direction of the force of gravity is changed step by step to make the angles $+\varepsilon$ and $-\varepsilon$ with the vertical, at the rate of the precession.

(e = charge of the electron = 1.6×10^{-19} Asec, m_0 = mass of the electron at rest = 9×10^{-31} kg, $eh/4\pi m_0 = 9.3 \times 10^{-24}$ A·m²).

Let us suppose that this minute electron magnet is placed in a constant magnetic field H. It will then first try to point with its north pole in the direction of H, thus tending to take up a position where the momentum is the minimum. The situation would then correspond to that of the spinning-top pendulum in fig. 2*a*.

We know, however, that when the axis of the spin makes an angle ϑ with the field the electron comes under the influence of a couple $M \sin \vartheta = \mu_B \cdot \mu_0 H \sin \vartheta$, as a result of which, like the case with the spinning-top pendulum in fig. 2*b*, the axis describes a precessional movement about the direction of H with an angular velocity

$$\omega_p = \frac{M}{J} = \frac{e}{m_0} \mu_0 H \quad . \quad . \quad . \quad . \quad . \quad . \quad (6)$$

Now it is easy to cause the direction of the magnetic field to oscillate over a small angle ε_1. All that need be done is to apply an alternating field

$$h\,(t) = \varepsilon_1 H \cos \omega t$$

perpendicular to H.

Calculation for a sinusoidal interference

Let us go back for a moment to the model of the spinning-top pendulum. We take the direction of the vertical as the z-axis of a rectangular system of coordinates and let the force of gravity oscillate in such a way that the z-component is a constant (value g) and the y-component remains zero, whilst the x-component, $u(t)$, becomes:

$$u\,(t) = \varepsilon_1 g \cos \omega t \qquad (\varepsilon_1 \ll 1)\,.$$

If, now, ξ and η represent the angles enclosed by the z-axis and the projections of the axis of the spinning-top on the XOZ and YOZ planes respectively (*fig. 5*) then as long as $\xi \ll 1$ and $\eta \ll 1$, and in the absence of frictional forces, we have

$$\frac{d\xi}{dt} = -\omega_p \eta, \quad . \quad . \quad . \quad . \quad . \quad . \quad . \quad . \quad . \quad (7)$$

$$\frac{d\eta}{dt} = \omega_p (\xi - \varepsilon_1 \cos \omega t) \quad . \quad . \quad . \quad . \quad . \quad (8)$$

These equations signify that the point (ξ, η), the point where the pendulum arm intersects a horizontal plane at a distance 1 below the point of suspension, is describing a circle around the point $(\mu, 0)$, i.e. the point where the direction of the force of gravity through the point of suspension intersects the said plane, and at a constant angular velocity ω_p. The point (ξ, η) must thereby always "follow" the variable point $(\mu,0)$.

The stationary solution of the equations (7) and (8) reads:

$$\xi = \frac{\omega_p^2}{\omega_p^2 - \omega^2} \varepsilon_1 \cos \omega t, \quad . \quad . \quad . \quad . \quad (9)$$

$$\eta = \frac{\omega_p \omega}{\omega_p^2 - \omega^2} \varepsilon_1 \sin \omega t\,. \quad . \quad . \quad . \quad (10)$$

Thus the axis of the spinning top describes an elliptical cone, the apex angles of which are greater according as the difference between ω and ω_p is smaller. When the value of ω lies very close to ω_p these formulae no longer hold, because then the values found for ξ and η are no longer $\ll 1$. It is to be noted that ξ is in phase with the interference $\varepsilon_1 \cos \omega t$, as a result of which no work will be performed by the alternating field on the spinning top. Thus there is no dissipation of energy, in accordance with the assumption made that frictional forces are absent.

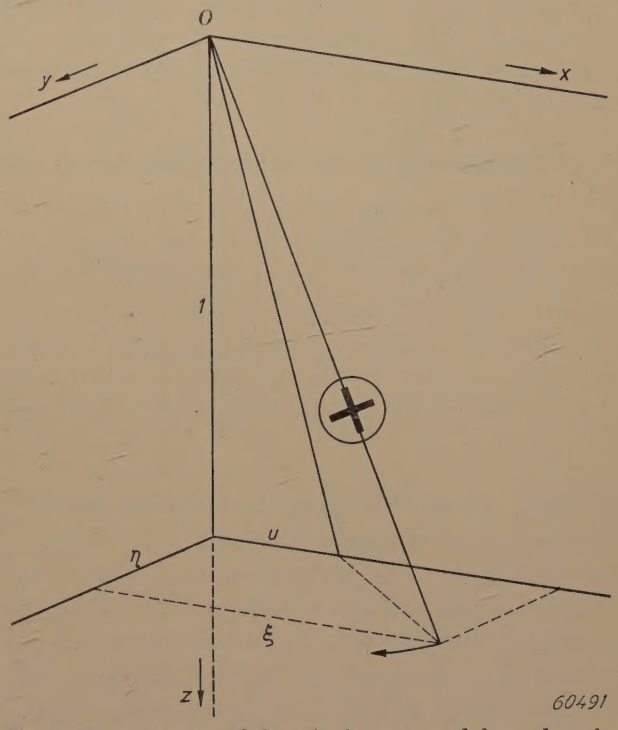

Fig. 5. The behaviour of the spinning-top pendulum when the direction of the force of gravity oscillates sinusoidally between $+\varepsilon_1$ and $-\varepsilon_1$.

When, in the case of the electron, we take H parallel to the z-axis of a rectangular system of coordinates and h parallel to the x-axis, a calculation shows that the components μ_x and μ_y of the magnetic moment of the electron in the x- and y-directions respectively are given by:

$$\frac{\mu_x}{\mu_B} = \frac{{\omega_p}^2}{{\omega_p}^2 - \omega^2} \varepsilon_1 \cos \omega t \quad . \quad . \quad . \quad (11)$$

$$\frac{\mu_y}{\mu_B} = \frac{\omega_p \omega}{{\omega_p}^2 - \omega^2} \varepsilon_1 \sin \omega t \, . \quad . \quad . \quad . \quad (12)$$

In these expressions we recognize the equations (9) and (10). Naturally, limitations similar to those applying in the case of the mechanical model also apply here ($\mu_x/\mu_B \ll 1$, $\mu_y/\mu_B \ll 1$, absence of damping).

From the formulae (11) and (12) it appears that under the given conditions an alternating magnetic field directed along the x-axis causes not only an alternating magnetic moment directed along the x-axis and in phase with the field, but also an alternating magnetic moment which is directed along the y-axis, thus perpendicular to the magnetic alternating field, and which lags 90° in phase behind that field.

Experimental evidence for the precessional movement

The following experiment [6]) directly proves the existence of the magnetisation component μ_y.

An arrangement of wave guides forming a so-called "magic tee", as indicated in *fig. 6*, is placed in an adjustable constant magnetic field H_z. A sphere of ferrite material is placed inside the wave guide *a-b*, in the origin of the system of coordinates x, y, z. A microwave ($\lambda = 3.2$ cm, $\omega = 2\pi \times 9.4 \times 10^9$ rad/s) enters at *c*.

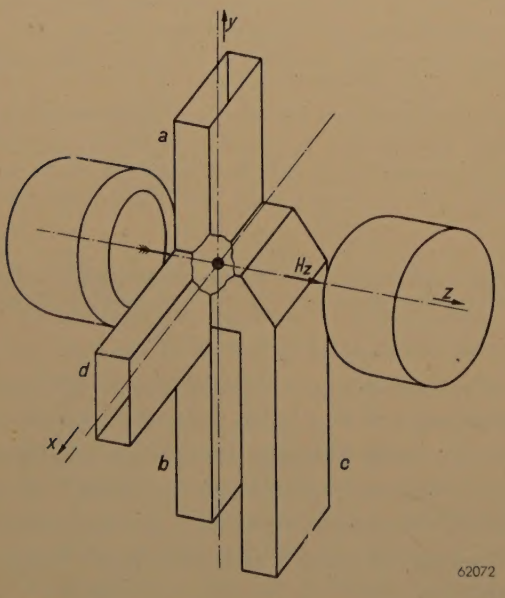

Fig. 6. The wave guides *a*, *b*, *c* and *d*, forming a so-called "magic tee", are placed in an adjustable constant magnetic field H_z. At the origin of coordinates a small sphere of ferrite is placed. A microwave enters at *c*. The fact that a wave is observed in *d* proves the existence of the magnetisation component in the "third direction" μ_y in the ferrite material.

[6]) H. G. Beljers, Physica The Hague, **16**, 75-76, 1950 (No. 1)

Let us first consider the case $H_z = 0$. Provided a rigorous symmetry of the whole arrangement is established (e.g. by adjusting the position of the sphere), the wave in *c* splits into equal waves travelling in *a* and *b*, but no wave is observed in the limb *d*. This is due to the fact that the possible mode of a wave in *d* can be launched only by an oscillating magnetic field component in the y-direction, while the arriving wave from *c* does not possess such a component. A wave in *d* is found, however, when the constant field H_z is given a finite value. This is explained by the gyromagnetic effect in the ferrite sphere, giving rise to a magnetization component in the "third direction", μ_y.

When H_z is varied the output measured in *d* shows a rather sharp maximum at $H_z = m_0/e\,\mu_0 \cdot \omega$, which is in agreement with eq. (6).

The formulae (11) and (12) derived above apply for a single, isolated electron and also, as the theory further shows, for a homogeneous, spherical, ferromagnetic body magnetized to the point of saturation by an external magnetic field. This is subject to the condition that the dimensions of the sphere are small in relation to the wavelength $\lambda = 2\pi v/\omega$, where $v = c/\sqrt{\varepsilon\mu}$ represents the velocity of propagation of electromagnetic waves in the ferromagnetic medium.

In a magnetic material of less symmetrical shape, for instance an ellipsoid, a somewhat different result is found for ω_p, namely:

$$\omega_p = (e/m_0)\,\mu_0\,[H + (N_x - N_z)M]^{1/2}\,[H + (N_y - N_z)M]^{1/2},$$

where M represents the magnetic moment of the body per volume unit (in A/m) and N_x, N_y and N_z are numerical factors determining the demagnetizing forces in the three principal directions. For a sphere $N_x = N_y = N_z = 1/3$, so that we again obtain formula (6) unchanged.

Influence of damping

Just as in the discussion of the case of exact resonance, in the formulae (9) and (10) no account has been taken of the damping which always exists in nature. Let us consider the case of a spinning-top pendulum making a precessional movement about the direction of minimum energy at an angle ϑ to the vertical, as in fig. 2*b*, and let there be a force which does not influence the speed of rotation of the spinning top but which tends to retard the movement of the pendulum — just as it would do in the case of an ordinary pendulum — and which is, let us say, proportional to the (precessional) velocity. Obviously such a frictional force reduces the energy of the pendulum and, since we are assuming that the spinning top itself continues to rotate at an undiminished velocity, as a result the centre of gravity must in time fall,

whilst further, in the absence of any external interference, the precession gradually comes to an end and the pendulum takes up its lowest position (as in fig. 2*a*).

In the case of an external interference $\varepsilon_1 \cos \omega t$ as dealt with above, such a frictional force will likewise make itself felt. It will result in the ultimate amplitude of the precession being smaller than the value given by (9) and (10) and the x-component lagging behind the interference. This gives rise to a continuous dissipation of energy, which, if the friction in question were caused, for instance, by a viscous medium, would result in that medium being heated.

In particular, in the case of exact resonance ($\omega = \omega_p$) the expression for the amplitude of the precession will no longer become infinite but will ultimately assume a finite value, so that the half-value width [7]) of the precession, which in the absence of damping is nil, has a value differing from zero.

Just as with the spinning-top pendulum, also in the case of the electron a damping force leads to a reduction of the amplitude and at the same time a relative widening of the magnetic resonance interval, accompanied by dissipation of energy. Such a damping cannot arise when an electron is free but it may well occur in the case of electrons forming part of a crystal. It will result, on the one hand, from interaction with the free electrons in the material and, on the other hand, from an interaction between the electron in question and the ions of the crystal lattice. The energy dissipation accompanying this leads to the crystal being heated (magnetic losses). Although, therefore, we have regarded the damping here more or less as a secondary phenomenon, it is of very great importance in practice.

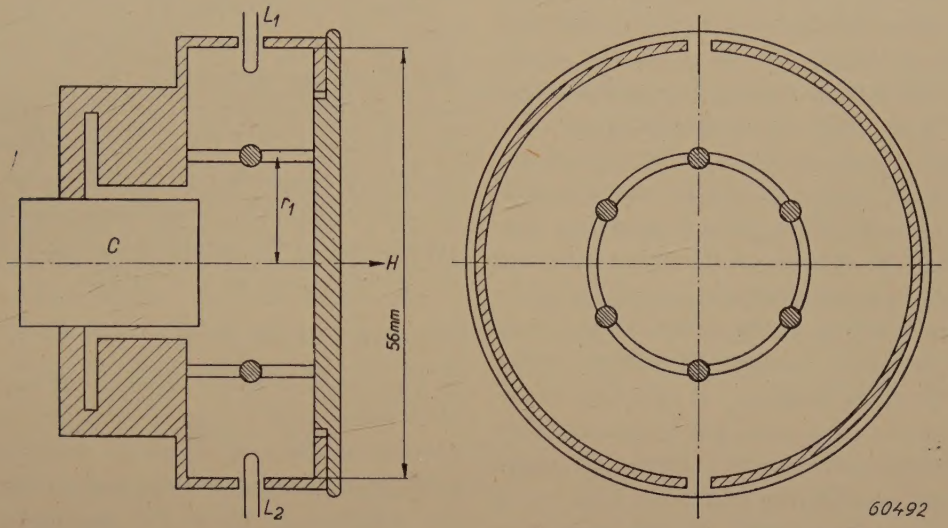

Fig. 7. Box-shaped cavity resonator for studying gyromagnetic resonance. The ferrite is applied in the form of small spheres on a cylinder of insulating material. The movable metal cylinder C serves for tuning. One of the two loops, L_1, serves for generating the oscillation energy and the other, L_2, for measuring it.

Further experimental study of magnetic resonance

For a closer investigation of the consequences of gyromagnetic resonance of ferrites, experiments were carried out with a cylindrical cavity resonator (*fig. 7*) containing small samples of ferrites at given places [8]). The magnetic material is introduced in the form of small spheres placed on a circle situated in a plane perpendicular to the axis of the box and at half its height. With the aid of a coupling loop passed through an opening in the side of the box it is possible to generate in the cavity resonator a standing electromagnetic wave of a frequency corresponding to a certain form of oscillation of the cavity resonator. The mode of oscillation and the radius of the circle mentioned above in relation to the dimensions of the cavity resonator can be so chosen that the magnetic vector h of the alternating field at the place where the spheres are situated lies in the plane of the circle and is tangential thereto, whilst

[7]) The half-value width is the difference between the two frequencies at either side of the resonance frequency for which the energy equals half the energy in the point of resonance.

[8]) H. G. Beljers, Measurements on ferromagnetic resonance using cavity resonators, Physica The Hague **14**, 629-641, 1948 (No. 10).

at the same time the electric vector at those points is just zero or approximately zero.

A constant magnetic field H is applied parallel to the axis of the box. Since the frequency of the cavity resonator, partly in connection with the above-mentioned requirements, is fixed (in the case investigated it was $f = 10^{10}$ c/s, $\omega = 2\pi f = 6 \times 10^{10}$ rad/sec), H has to be so chosen that according to formula (6) ω_p comes to lie round about ω (in our case $\omega_p = \omega$ when $H = 3 \times 10^5$ A/m or $\mu_0 H = 0.4$ Wb/m^2).

In the bottom of the box is a movable, threaded metal cylinder C, by means of which the cavity resonator, the natural frequency of which depends partly upon the presence of the magnetic material, can be brought to resonance at the fixed frequency ω. The presence of such a resonance can be determined with the aid of a second coupling loop inserted through an opening in the side of the box in the same way as is done with the driving loop. The influence of the presence of the ferrite in the box is then studied by first tuning the empty cavity resonator to the fixed frequency ω and then determining how far the cylinder C has to be moved in order to bring the cavity into resonance again at the frequency ω after the ferrite has been put in place and the field H imposed. At the same time measurements are taken, in the known manner, of the resonance width, and thus of the reduction in quality of the cavity resonator.

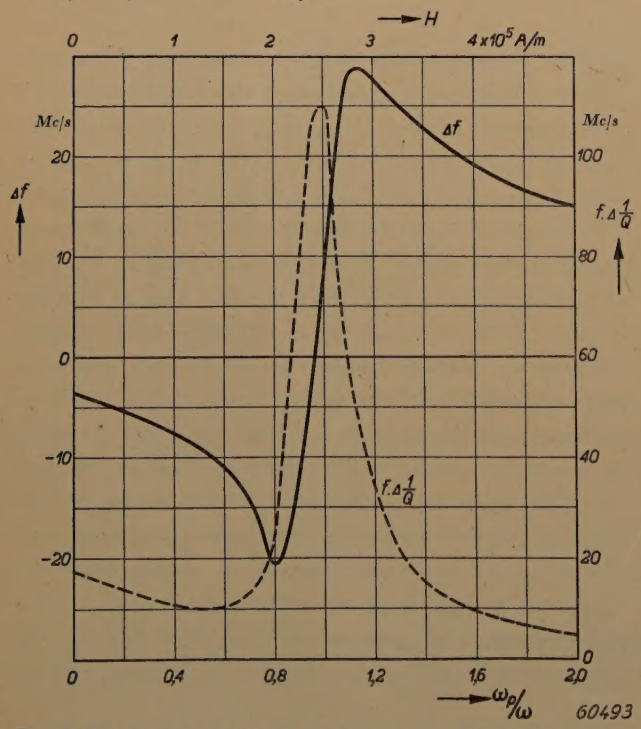

Fig. 8. The detuning Δf of the cavity resonator and the quantity $f \cdot \Delta(1/Q)$ as functions of the field strength H and of the quantity ω_p/ω respectively (ω is the practically fixed angular frequency of the cavity resonator).

Let x be the reading obtained when C is in a certain position. Then, in the absence of the ferrite, with a certain reading x_0 one will find a sharp resonance with the fixed frequency ω. When ferrite is present and at the same time a homogeneous magnetic field H is applied parallel to the axis of the box, resonance is found when C gives a reading x_1. The quantity $x_1 - x_0$ is a measure for the detuning of the cavity resonator due to the gyromagnetic effect. One can also determine the readings x_2 and x_3 of C where the energy, with the drive kept constant, is half as great as that for the reading x_1. The quantity $x_2 - x_3$ is then a measure for the quality of the cavity resonator when this is affected by the presence of the ferrite.

In *fig. 8* the detuning Δf, i.e. the frequency change which the displacement of the body C would have caused in the case where the box is empty, has been plotted on the left as a function of H, whilst the change $f \cdot \Delta(1/Q)$ — where Q represents the quality of the cavity resonator — has been plotted on the right. The quantities Δf and $f \cdot \Delta(1/Q)$ correspond to the quantities μ_r' and μ_r'' introduced at the beginning of this article.

Discussion of the results

The trend of both these functions answers the theoretical expectation if allowance is made for a certain amount of magnetic damping. As in the first experiment described (fig. 6), the value of ω_p for which $f\Delta(1/Q)$ is the maximum ($\omega_p = \omega = 5.8 \times 10^{10}$ rad/sec) agrees well with the value which, according to formula (6), follows from the corresponding value of H (2.5×10^5 A/m), namely 5.6×10^{10} rad/sec.

It appears that the general trend of the curve as found from experiments agrees with formula (11) for μ_x/μ_B if we add to that formula the damping term $jd\omega$, thus:

$$\frac{\mu_x}{\mu_B} = \frac{\omega_p^2}{\omega_p^2 - \omega^2 + jd\,\omega}\,\varepsilon_1\, e^{j\omega t}.$$

The real part of this expression is proportional to $x_1 - x_0$, the imaginary part to $x_2 - x_3$. It appears that for $\omega_p > \omega$ the real part increases as ω_p decreases and rather suddenly changes sign when the quotient ω_p/ω becomes less than 1. The peak value for $(x_2 - x_3)$ is a measure for the gyromagnetic damping factor d, in that the smaller the value of d the greater is this peak value (thus the maximum decrease in quality of the cavity resonator).

For a study of the gyromagnetic losses it is desirable to know the trend of μ_r' and μ_r'' as a function of ω or of $f = \omega/2\pi$ with a constant field H, and preferably for small values of H. It is very tempting to read fig. 8 — where a scale is also given for the ratio ω_p/ω (where ω_p is proportional to H, and ω represents the fixed frequency of the cavity resonator) — from right to left and to regard ω_p as a constant and ω as a variable frequency. Since in the formulae (11) and (12) the ratio ω_p/ω occurs as

the only variable factor, figure 8 would then have to apply for an arbitrary value of ω_p. However, this is not permitted, because the damping, which has not been taken into account in the formulae (11) and (12), is a function of ω that presumably increases strongly with diminishing ω, in a manner so far unknown.

Therefore, until further experiments have been made (with smaller values of ω and with correspondingly smaller values of ω_p and thus of H) nothing can be said about this with any certainty. But it is possible to predict qualitatively what is to be expected. With constant H and increasing ω first an increase of μ_r' is to be expected, followed by a sharp decline, whereby μ_r' may even become negative. In the interval where μ_r' is already falling there will be a sharp rise in μ_r'', after which it will likewise pass through a maximum. This is exactly in accordance with the behaviour found for various ferrites according to fig. 1 when there was no constant magnetic field present; only the maximum of μ_r' is not very clear there and no negative values of this quantity are found. This will be considered somewhat more closely in what follows.

Resonance in the absence of a constant external field

We revert to the losses occurring in ferrites at frequencies of about 10^6 c/s and higher when these ferrites are not placed in a constant external magnetic field.

In the case of a material that is not placed in an external field and in which the losses are therefore measured in the usual way, it must be borne in mind that gyromagnetic resonance may still play a part, since in a magnetic material there are always some internal forces present which tend to give certain directions to the spinning vectors [9]). The greater these anisotropic forces the more difficult it is to change the direction of the spinning vectors, and thus the smaller will be the permeability μ_r. Although these coercive forces need not necessarily be of a magnetic nature, it may be assumed that they are capable of causing a precession of the spinning vectors, just like an external field H. Expressing these forces as an equivalent field H that would cause the same coercive effect, we arrive at values of 10^{-3} to 10^{-2} Wb/m^2 for $\mu_0 H$, corresponding to a frequency $\omega_p/2\pi$ of 2×10^6 to 2×10^7 c/s. This does indeed already bring us very close to the frequency range in which the phenomena described in the beginning of this article occur. The fact, expressed in fig. 1, that the abnormal behaviour of μ_r' and μ_r'' occurs at higher frequencies according as μ_r' is smaller in the low-frequency range, agrees well with what has just been stated, namely that a small value of μ_r signifies strong anisotropic forces, thus a high value of the equivalent H and the corresponding ω_p.

The fact that the ageement of the curves of fig. 1 with fig. 8 read from right to left is only qualitative, and that the abnormal behaviour of μ_r'' already begins at frequencies which are still a factor 10 or 20 smaller than what follows from the estimation made by means of the anisotropic forces, is most probably to be ascribed to the internal stresses in the material. The accompanying internal field strengths may weaken or compensate the anisotropic fields locally, resulting in a general widening of the resonance figure and a flattening of the maxima.

An analysis shows that for forces originating from elastic stresses the magnetic energy, which in the case of an external field H_p assumes the form

$$E = \tfrac{1}{2} H_p \Theta^2 ,$$

in which Θ is the angle of magnetization by H_p (assumed to be small), is often to be generalized to the expression

$$E = \tfrac{1}{2} (H_x \Theta_x^2 + H_y \Theta_y^2) ,$$

in which H_x and H_y are the "effective fields" for deviations in the x and y directions respectively. It is easily calculated that in that case the resonance frequency ω_0 assumes the form:

$$\omega_0 = \gamma (H_x H_y)^{1/2}, \text{ in which } \gamma = \frac{e}{m_0} \mu_0 .$$

For stresses of a special type H_y may, for instance, sometimes be zero, and then this leads in principle to a resonance frequency zero. It will not be so bad as this in practice, but still it is to be expected that certain parts of the material will have a lower resonance frequency than others [10]).

To sum up, it may be said that a deeper insight has been obtained into the nature of the losses occurring in ferrites at high frequencies, but that it is not yet possible to account for all the details of the phenomena observed. The future will certainly show some progress, in which the perfecting of the material itself will play a part.

The gyrator

Finally, attention is drawn to a possibility of making use of the gyromagnetic effect for constructing a so-called gyrator.

In the foreging (see equations (11) and (12)) it has been shown that the gyromagnetic resonance differs from the normal resonance in that an alternating field in the x-direction

[9]) See, e.g., J. J. Went, Philips Techn. Rev. **10**, 246-254, 1948 (No. 8).

[10]) See J. L. Snoek, Physica The Hague **14**, 207-217, 1948 (No. 4).

causes an alternating polarization not only in the x-direction but also in the y-direction, thus at right angles to it. This alternating polarization, which has also been observed experimentally, can be used in electro-technical engineering.

When an alternating current passes through a coil the axis of which is parallel to the x-axis of a system of coordinates then, without the presence of ferrite, no voltage is induced in another coil the axis of which is parallel to the y-direction. When, however, there is in the field a material which shows gyromagnetic resonance and is magnetized in the z-direction then a voltage will indeed be induced in the latter coil. Tellegen [11]) has shown that such a combination of two crossed coils forms a four-terminal network, called a gyrator, differing from the known four-terminal networks, such as the transformer, in that it does not comply with the law of reciprocity (the law of reciprocity for an electrical network states that the current in one branch of this network, generated by an alternating voltage in another branch, corresponds in amplitude and phase to the current generated in the latter branch as a result of an equally large alternating voltage in the branch first mentioned). Two of such four-terminal networks connected in cascade form a four-terminal network obeying the law of reciprocity. We cannot here enter further into the interesting practical possibilities offered by this new element for electrical networks.

[11]) B. D. H. Tellegen, The gyrator, a new electric network element, Philips Res. Reports **3**, 81-101, 1948 (No. 2).

Summary. The material named "Ferroxcube" is characterized by very low eddy-current and hysteresis losses. In the frequency range of 0-10^5 c/s some after-effect is observed. Above a certain critical frequency, differing between one material and another, additional losses occur which may be ascribed to gyromagnetic resonance. The theory of this phenomenon is explained with the aid of a mechanical model. Further, measurements of the gyromagnetic resonance are described which have been carried out with a material placed in a constant, strong magnetic field polarizing the material in a direction perpendicular to the direction of observation. These measurements confirm in the main the theoretical expectation. It is indicated briefly how the losses observed can be explained qualitatively from the gyromagnetic phenomena. Finally it is pointed out that with the aid of gyromagnetic effect a four-terminal network with new properties (a gyrator) can be constructed.

THE MANUFACTURE OF QUARTZ OSCILLATOR-PLATES

I. HOW THE REQUIRED CUTS ARE OBTAINED

by W. PARRISH *).

549.514.51:621.396.611.21

The quartz plate as used for the frequency control of radio transmitters is a device requiring extreme precision in its preparation. The manufacture of such plates is an interesting problem, especially so when mass production is envisaged. This problem was tackled and solved in an impressive way by the United States during the war employing the combined efforts of crystallographers, physicists, experts in electronics, mechanical engineering and allied fields.

Among the more than 100 factories which took part in the mass production, the North American Philips Company was able to make several not unimportant contributions to the development of the methods of manufacture. These contributions, as well as the development referred to in general, have been described since the war in various American periodicals. Nevertheless the editors of this Review feel that it may still be of interest to many readers, especially non-Americans, to learn something about these methods of manufacture.

Introduction

In 1921 W. G. Cady showed that the vibration of a plate cut from a piezo-electric crystal such as quartz may serve to control the frequency of a vacuum tube oscillator. This method gradually found its way into the practice of short wave radio transmitters. Thus, for example, in the United States in 1939 about 50,000 quartz plates were manufactured for this purpose.

World War II gave a strong impulse to short wave communication technique. Upon the entrance of the United States into the war a program was set up in that country which provided for the equipment of huge numbers of aircraft, tanks, small infantry units, etc., with a transmitting-receiving apparatus. The use of quartz oscillator-plates made possible precise frequency control and push-button tuning on a scale never before attempted. The production of quartz oscillator-plates rose from about 100,000 in 1941 to about 6 million in 1942 and then to about $28^1/_2$ million in 1944. The following is a rough breakdown of the last figure [1]): 8 million oscillator-plates were made for aircraft, $4^1/_2$ million for tanks and artillery units, 11 million for walkie-talkies and handie-talkies, the rest for various vehicles and naval vessels. At the end of the war the production rate increased to about 60 million per year and the price had dropped to only a small fraction of pre-war prices.

This rapid rise in the production of quartz plates was based on the development of methods of manufacture which are interesting because of the remarkable combination of extreme precision required, with the speed and simplicity made necessary by wartime demands and limitations. A concise, but practically complete survey of these manufacturing methods was published in a symposium of the Mineralogical Society of America [2]) in the early part of 1945. In this periodical we must restrict ourselves to several phases of the manufacturing process, viz., those in whose development the Philips concern, in particular the crystal factory at Dobbs Ferry, the X-ray factory at Mt Vernon and the laboratory at Irvington, have had an active part. This article will give a broad survey of the problem of cutting the quartz plates out of the natural raw crystals; in a subsequent article a discussion will be given of the accurate determination of the

*) Philips Laboratories, Inc., Irvington-on-Hudson, New New York, U.S.A.

1) See: C. Frondel, History of the quartz oscillator-plate industry 1941-1944, Amer. Mineralogist **30**, 205-213, 1945.

2) The symposium number of the American Mineralogist (May/June 1945) contains in addition to the article quoted in footnote 1) the following:
K. S. van Dyke, The piezo-electric quartz resonator (p.214-244).
R. E. Stoiber, C. Tolman and R. D. Butler, Geology of quartz crystal deposits (p. 245-268).
S. G. Gordon, The inspection and grading of quartz (p. 269-290).
J. S. Lukesh, The effect of imperfections on the usability of quartz for oscillator-plates (p. 291-295).
W. Parrish and S. G. Gordon, Orientation techniques for the manufacture of quartz oscillator-plates (p. 296-325).
W. Parrish and S. G. Gordon, Precise angular control of quartz-cutting by X-rays (p. 326-346).
W. Parrish and S. G. Gordon, Cutting schemes for quartz crystals (p. 347-370).
W. Parrish, Methods and equipment for sawing quartz crystals (p. 371-388).
W. Parrish, Machine lapping of quartz oscillator-plates (p. 389-415).
C. Frondel, Final frequency adjustment of quartz oscillator-plates (p. 416-431).
C. Frondel, Effect of radiation on the elasticity of quartz (p. 432-446).
C. Frondel, Secondary Dauphiné twinning in quartz (p. 447-460).

desired cutting directions with the help of a special X-ray diffraction apparatus designed by Philips; a third article will treat the methods employed in lapping and finishing the oscillator plates.

The reader who would like to refresh his memory of several general concepts in the field of the application of the piezo-electric effect should refer to a short survey article [3]) which appeared in this periodical several months ago and to Heising [4]) and Cady [5]).

Low temperature coefficient cuts

The resonance frequency of a quartz plate of given dimensions and vibrating in a given mode of oscillation depends upon the temperature. This dependence may be very slight in certain temperature ranges, when the crystallographic axes of the plate make certain, accurately determined angles with the boundaries of the plate. This is usually formulated the other way round: it is said that the oscillator plate must be cut from the crystal at definite angles to the crystallographic axes of the crystal. Examples of these "low temperature coefficient cuts" are the AT, BT, GT cut, etc.

It is obvious that quartz plates cut to be independent of temperature should be preferred for radio transmitters. The object of using such plates is the stabilization of the transmitter frequency, and by the use of the cuts in question, without the necessity of a thermostat for the quartz plate, the frequency is made also highly insensitive to variations in the temperature of the surroundings, which e.g. in aircraft may be very great. The low value of the temperature coefficient with these cuts is obtained only in a limited temperature range: the resonance frequency as a function of temperature passes through a maximum (or through a flat turning point). Optimum frequency stability is realized by operating the crystal around the temperature of this maximum. The broadness of the maximum, i.e. the width of the useful temperature range, depends on the type of cut. In the case of the often used BT cut the frequency does not vary more than 0.02 % in a temperature range of about 140 °C. With other cuts an even greater constancy of frequency can be obtained.

The various cuts differ in the oscillation mode for which the temperature coefficient becomes small. As the resonance frequency of a plate vibrating in a given mode chiefly depends on its dimensions, and as it is not practicable to make the plates either very thin and small or very large, each cut has a specific frequency range in which it can be used. Furthermore there is the difference in width and position of the useful temperature region. A further factor in the choice of cut to be employed is the degree to which undesired modes of oscillation (with nearby resonance frequencies) are excited by the desired vibration. This would lead to an extra damping, decrease of "activity" at some frequencies, heating of the plate and other disturbing effects. Roughly it may be said that in the frequency regions of 2-5 Mc/sec only AT cuts and of 5-9 Mc/sec only BT cuts are employed, both vibrating in the fundamental thickness shear mode shown in *fig. 1*. For frequencies up to 100 Mc/s

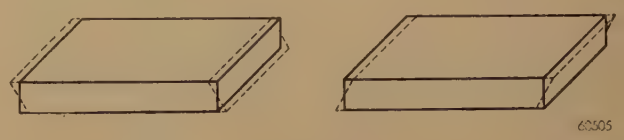

Fig. 1. AT an BT cut oscillator plates are used in a thickness shear vibration mode. The deformation involved in this mode is indicated by dotted lines.

AT- or BT-plates vibrating in higher harmonics of this mode are used. With the BT-cut the useful temperature region can be varied within limits by changing the cutting angle of the plate with respect to the optic axis. For example, a change of 30 minutes of arc in cutting angle may shift the useful range as much as 10-20 °C.

The slightness of this angle variation gives at the same time an idea of the high precision required in the orientation of the plates. As to the thickness of the plates, the tolerances there are also extremely small; the plates for two communication channels adjacent to each other in frequency may for example differ in thickness by as little as one ten-millionth of an inch.

What is now the position in the quartz crystal of the different low temperature coefficient cuts?

Quartz crystallizes in the symmetry class D_3 (Schoenflies notation) which possesses one threefold axis of symmetry and perpendicular to that three twofold axes of symmetry. Some of the faces which may be found on a freely growing quartz crystal are shown in *fig. 2*. The vertical axis Z is the threefold, so-called optic axis. The six side faces parallel to Z are called the prism faces (m). The three horizontal twofold axes X, each of which is parallel to two prism faces, are the so-called electric axes. For the sake of completeness we

[3]) J. C. B. Missel, Piezo-electric materials, Philips Technical Review **11**, 145-150, 1949 (No. 5).
[4]) R. A. Heising, Quartz crystals for electrical circuits, Van Nostrand, New York 1946.
[5]) W. G. Cady, Piezoelectricity, McGraw-Hill, New York 1946.

also mention the three intermediate horizontal axes, the *Y*-axes, each perpendicular to an *X*-axis (and therefore perpendicular to the prism faces). The crystal boundaries at the pyramidal ends of the crystal drawn are formed chiefly by the three

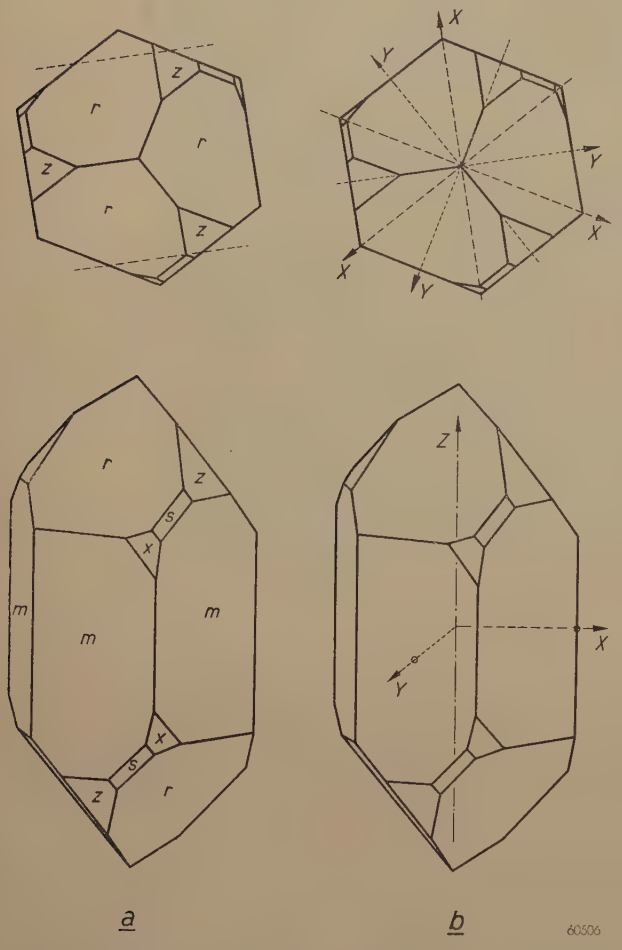

Fig. 2. Ideal quartz crystal. In (*a*) the customary indications for the various faces are given; *m* are the prism faces, *r* major and *z* minor rhombohedron faces. In (*b*) the directions are given of the *Z*-axis (optic axis), the three *X*-axes (electric axes) and the three *Y*-axes.

The dotted lines in (*a*) above are the cutting lines along two planes parallel to *X* and *Z*, as described in the first step of the *X*-block method of cutting the quartz crystal.

so-called major rhombohedron faces, indicated by *r*, the three so-called minor rhombohedron faces, indicated by *z*, and the small faces *s* and *x*.

Most of the low temperature coefficient cuts developed until now are parallel to one of the *X*-axes and therefore perpendicular to a *Y*-*Z*-plane. They differ only in the angle which they make with the *Z*-axis. In *fig. 3*, which shows a cross section of the crystal in the *Y*-*Z*-plane, these cuts are indicated. They are all perpendicular to the plane of the drawing, like the rhombohedron faces *r* and *z* crossed by the section shown. It may be seen that the AT and the BT cuts, in which we are mainly interested, run roughly parallel to a *z* and an *r* face, respectively.

The orientation of the crystals under the saw

The quartz crystals found in nature usually have little resemblance to the ideal crystal drawn in fig. 2. *Fig. 4* shows several natural crystals. On these crystals some prism and rhombohedron faces may be seen and the type of face can in general readily be established, since the angles between faces are always the same. But the various faces are by no means developed to the same extent, so that the crystal does not in general show any macrosymmetry. Crystals are frequently found which show no clear boundary faces at all (defaced crystals).

In such a more or less irregular crystal the determination of the planes along which it must be sawed, e.g. for an AT cut, is made possible with the required very small tolerances by two fundamental means: the phenomena of double refraction and X-ray diffraction. The way in which these means, along with other ones (as the natural faces on the crystal and the light figures on etched surfaces), are applied can most easily be explained by following in detail one of the several cutting methods. For that purpose we have chosen the

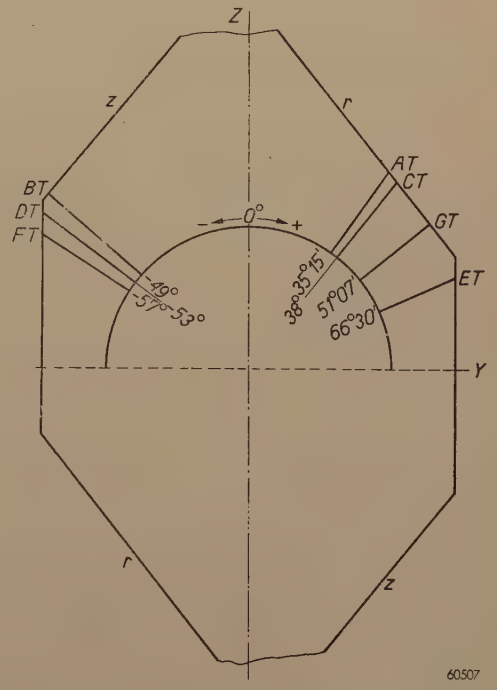

Fig. 3. Cross section of a quartz crystal parallel to a *Y*-*Z*-plane (i.e. perpendicular to an *X*-axis). Most of the low temperature coefficient cuts are perpendicular to this cross section, at angles with the *Z*-axis as indicated here. AT, CT, GT and ET cuts are roughly parallel to the *z* face, and BT, DT an FT cuts roughly parallel to the *r* face.

Some oscillator plates are made circular or rectangular but most are made square. One side is then perpendicular to the plane of the drawing (thus parallel to *X*), except in the case of the GT cut, where the sides must make angles of 45° with this plane. The length of the sides varies between 0.1 and 2 inches, a normal value being 0.5 inch.

Fig. 4. Several typical natural quartz crystals. Top, two defaced crystals; the one on the left was rolled around in a stream bed in nature and natural faces abraded off, whereas the faces of the crystal on the right were cobbed off at the mines to remove defective parts. Lower, three faced crystals; the one in the middle is set with the optic axis vertically to show the hexagonal outline while the crystals on the sides are "candle" shape with optic axis parallel to plane of photograph. (This shape with prism faces not parallel to the *Z*-axis is caused by these faces not being perfectly smooth but having a very fine step-like structure, composed of alternating prism and rhombohedral faces.)

so-called *X*-block method, which is the most generally successful method for crystals weighing less than about 1000 gms.

Suppose that the crystal to be sawn, although irregular, possesses at least one well developed prism face (*m*). First, a plane perpendicular to this prism plane and parallel to the *Z*-axis is cut at either side of the crystal. The planes cut are parallel to a *Y*-*Z*-plane (cf. *fig. 5*). The "*X*-block" thus obtained is placed on the table of the quartz saw

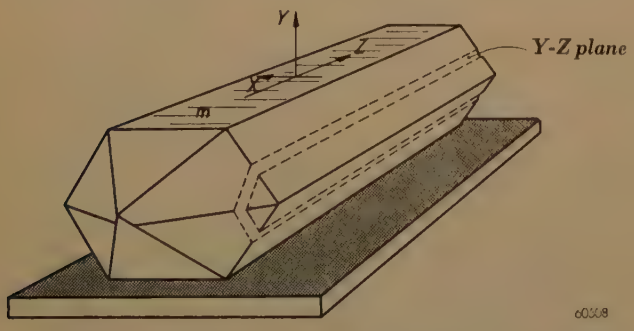

Fig. 5 When cutting crystal blocks according to the *X*-block method, preliminarily planes perpendicular to a prism face and parallel to the *Z*-axis are cut from both sides of the block. These are *Y*-*Z* planes (parallel to the cross-section in fig. 3).

(*fig. 6*) so that the saw blade is perpendicular to the *Y*-*Z*-planes, cut previously, and thus parallel to an *X*-axis of the crystal. According to fig. 3 it is now only necessary to rotate the crystal about this *X*-axis until the angle between the *Z*-axis and the saw blade has the value required for the type of cut and indicated in fig. 3. One may then saw a wafer out of the crystal (*fig. 7*), of the thickness desired for the oscillator-plates (plus the necessary extra thickness for lapping), and this wafer may then be cut into a number of oscillator-plates.

It is seen that in order to obtain the desired low temperature coefficient cut by this method two different orientations of the quartz crystal with respect to the saw are involved:

In the first orientation, for cutting a *Y*-*Z*-plane, the plane of the saw must be set perpendicular to the prism face and parallel to the *Z*-axis of the crystal. This is accomplished as follows. The crystal is placed with the well-developed prism face on a thick glass plate with a ground reference edge. On the saw table the glass plate can be fastened with the help of a reference edge on the table so that the

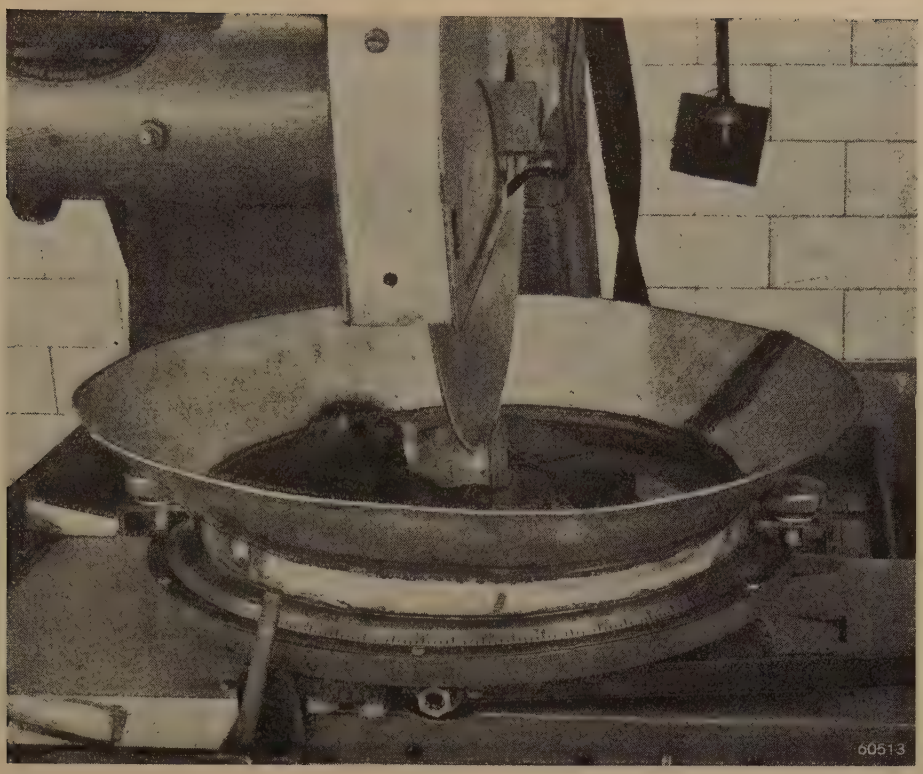

Fig. 6. Arrangement of a circular saw for sawing quartz crystals. A commonly used type of saw blade consists of sintered bronze containing diamond powder. The disc rotates with a peripheral velocity of about 30 m/sec, and can cut a surface area of for instance 30 cm^2 in two to three minutes. The quartz block is placed on the saw table, which can be rotated around a vertical axis and tilted around a horizontal axis; for this purpose the circumference is provided with a scale division in degrees. Moreover the mounted quartz block can be displaced parallel to itself over a distance in order to saw a series of parallel wafers of a given thickness out of the block.

reference edge on the glass is parallel to the saw blade. This gives the desired orientation, provided the crystal was placed on the glass plate in such a way that the *Z*-axis is exactly parallel to the reference edge [6]). A rough degree of parallelism can usually be accomplished by eye. The setting is then improved with the help of a simple instrument, the staurоscope (see *fig. 8*): in this instrument a beam of light travels perpendicularly through the glass plate and the crystal mounted on it while the crystal lies between crossed Polaroids. In the absence of the crystal there would be complete extinction; due to the double refraction of the crystal perpendicular to the optic axis a certain transmission of light is obtained, unless the "main directions" of the crystal (in this case the *Z*-axis and *X*-axis) are parallel to the directions of polarization of the Polaroids. Since the reference edge of the glass plate is set parallel to one of these directions of polarization by means of a reference edge on the instrument stage, by shifting the crystal slightly until extinction is re-established, the *Z*-axis can be made parallel to the reference edge with an accuracy of about 1°. In this position the crystal is cemented to the glass plate and a plane is cut from one side of the block. This, however, does not yet conclude the first orientation, since the accuracy mentioned is not sufficient. The X-ray method must now be applied to the cut surface enabling the crystallographic angles of the plane to be determined with an accuracy of a few minutes. The necessary corrections in the position

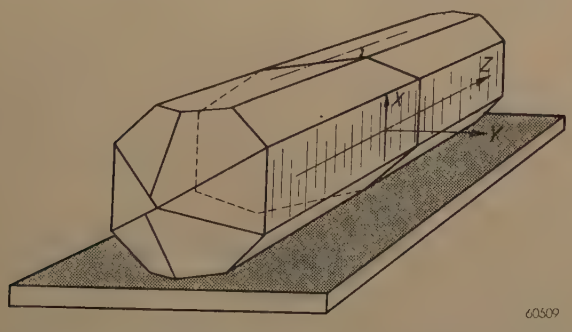

Fig. 7. *X*-block, that may be cut into wafers of one of the types of low temperature coefficient cuts shown in fig. 3. The saw blade is placed perpendicular to the freshly cut *Y*-*Z* top and bottom faces; it is then parallel to an *X*-axis. The crystal block is turned around this *X*-axis in order to obtain the desired angle between the saw blade and the *Z*-axis.

[6]) The method is not impaired by a "candle" shape of the crystal. In that case the prism face used is not perpendicular to a *Y*-axis, but it is only the parallelism of the face to an *X*-axis that matters. It is therefore even possible to use a rhombohedral face instead of a prism face in the mount for making an *X*-block.

of the crystal with respect to the saw blade can be deduced very simply from this and then realised by rotating (and if necessary slightly tilting) the saw table, whose circumference is provided with a degree scale with vernier reading. Again a plane is cut and X-ray tested, and if necessary a second correction must be applied. Usually, however, after the first correction the cut is already inside the tolerances of 15′ to 30′ parallel to the *Y*-*Z*-plane.

The *Y*-*Z*-plane at the other side of the mounted crystal block is cut in exactly the same way.

The second orientation described above consists in bringing the plane of the saw into a position perpendicular to the *Y*-*Z*-plane, and at the desired angle with the *Z*-axis. The first is accomplished by mounting the *X*-block, after it has been removed from its glass plate, with one of the fresh cut *Y*-*Z*-planes on another glass plate, again with the *Z*-axis parallel to the reference edge. After the plate has been fastened to the saw table the desired angle with the *Z*-axis is obtained by rotating the saw table into the position required, which can be read off on the degree scale of the table. In doing this, however, it is necessary to know whether to turn to the right or to the left. In fact, fig. 3, the cross section perpendicular to an *X*-axis in which the low temperature coefficient cuts have been indicated, could also be viewed from the other side: in that case left and right are reversed. Therefore, when examining an *X*-block it is necessary to ascertain the position of the *r* and *z* faces; then the rule can be applied that the AT cut is approximately parallel to *z* and the BT cut approximately parallel to *r*. The identification of *r* and *z* is quite easy by the method of etch figures. The crystal is etched in a concentrated water solution of ammonium bifluoride. When one cut surface of the etched *X*-block is placed over a point source of light one sees an unsymmetrical light figure on the top cut surface (due to refraction and reflection in the myriads of etch pits), from whose orientation the directions of *r* and *z* can immediately be deduced. This is explained by *fig. 9* [7]).

Fig. 8. Stauroscope. With the help of this instrument the *Z*-axis of a quartz block is made parallel to the reference edge of the glass holder. (The instrument shown is produced by The Polarizing Instrument Co., Inc.)

The adjustment to the required angle between *Z*-axis and saw blade by means of the scale division on the saw table is not accurate enough. Here also a test cut is made, the X-ray method applied to it for exact determination of the crystallographic angles actually obtained and the necessary corrections deduced. The tolerances here are 10′ to 15′.

When a test cut finally has been made which satisfies the requirements the crystal is sliced into wafers parallel to the test cut and about 1 to 1.2 mm in thickness. With poorly constructed saws, after each three or four cuts the orientation must be checked and if necessary corrected again.

The wafers obtained (see *fig. 10*) have two edges remaining from the *Y*-*Z*-planes which are accurately perpendicular to the *X*-axis. The square AT and BT oscillator-plates must also possess two sides perpendicular and two sides parallel to the *X*-axis

[7]) The ambiguity in viewing fig. 3 can also be eliminated by the statement that in the quartz crystal considered the positive direction of the *X*-axis, to which the cross section drawn is perpendicular, must point towards the observer. To this corresponds a method which was formerly used to solve the question about the direction of rotation, viz. by direct determination of the polarity of the *X*-axis by an electrical method. The crystal was compressed in the *X*-direction and the side was ascertained on which the charge caused by the piezo-electric effect was positive. This method is not only more elaborate than the one described in the text but it also has the disadvantage that it can in some cases be subject to serious errors entailing the loss of valuable material. This will be explained later (footnote [8])).

and it is therefore quite simple to mark off the desired blanks on the wafers and cut them out (see *fig. 11*).

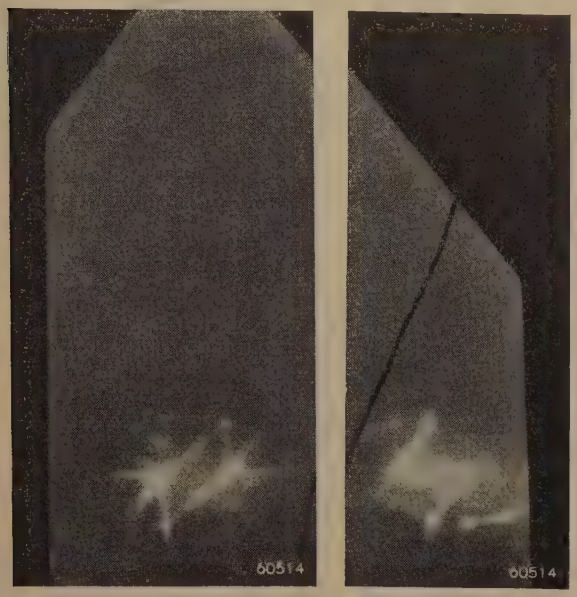

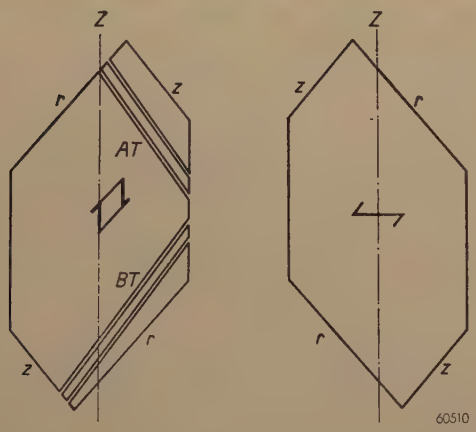

Fig. 9. *a*) Light figures observed when an etched *X*-block is placed over a point source of light and this source is viewed through the etched *Y*-*Z* plane. The parallelogram figure on the left is seen when the positive *X*-direction points towards the observer, and the reversed N figure appears when the negative *X*-direction points to the observer.
b) From the parallelogram figure the direction of the *r* and *z* faces can immediately be deduced and thus also the required direction of rotation of the *X*-block on the saw table. (The correlation as drawn here is independent of whether the quartz is right or left hand; see later.)

Cutting strategy

The above description still does not give the reader a good picture of the process of cutting quartz crystals because a very important complication has not been considered — a complication which overshadows the whole process, that is, twinning in natural crystals.

In a single quartz block, even one having practically the ideal shape of fig. 2, two or more crystals differing from each other in certain respects may be grown together. In the case of quartz there are

Fig. 10. A quartz block cut into wafers on its glass-holder. The photograph gives an idea of the large percentage of weight of quartz which is lost due to the thickness of the saw blade. It is furthermore of importance to note that the upper face of the quartz block, in the *X*-block method here used, is horizontal. With cutting methods where this is not the case there is a disturbing tendency of the saw blade to drift when entering the slanting surface, thus making the angles inaccurate.

two types of such twinning: electrical (Dauphiné twins) and optical (Brazil twins).

If we rotate the crystal cross-sectioned in fig. 3 180° around the *Z*-axis, the positive directions of all *Y*- and *X*-axes will point in the opposite directions, but the faces which exchange places in the figure make the same angles with the *Z*-axis. Two crystal individuals rotated in this way with respect to each other can therefore grow together without the intergrowth necessarily being visible to the eye: the faces *m* and *r* of the one individual are then "coplanar" with the faces *m* and *z*,

Fig. 11. Quartz wafer on which the blanks to be cut out are indicated with a rubber stamp. The straight edges on top and bottom of the wafer remaining from the *X*-block stage are perpendicular to an *X*-axis and are used as an accurate guide in cutting the blanks from the wafer. On the whole wafer and the separate blanks, the *X*-axis and the positive direction of the projection of the *Z*-axis (cf. the arrow heads) are indicated for later control measurements of the crystallographic angles of each oscillator plate. The determination of the *Z*-direction is carried out with an instrument similar to that of fig. 8 (angular view stauroscope).

respectively, of the other. This is called an electrical twin. It can sometimes be recognized by the occurrence of extra *s* and *x* faces and by other minor morphological features. The boundaries between the two or more individuals in an electrical twin are generally irregular as shown in *fig. 12*.

The symmetry class D_3 to which quartz belongs possesses no plane of symmetry. If the crystal drawn in fig. 2 is mirrored at any plane through the *Z*-axis, a crystal is obtained which is not identical with the original one, i.e. cannot be made to coincide with it by rotations and/or translations, but which nevertheless possesses all the properties of the first and is thus a possible crystal form of quartz. The two crystal modifications are in the same relation to each other as a right- and left-rotating threedimensional system of coordinates (or like a right and left glove). A crystal of the left-hand modification can grow together with one of the right-hand modification in such relative positions that the *Z*-axes are parallel and every *r* face of the one is parallel to a *z* face of the other. This is optical twinning, called thus, because the twins may be distinguished optically: they rotate the plane of polarization of a light beam in opposite directions. The boundaries between the two or more optical twins are always plane (parallel to an *X*-axis) and remarkably straight-edged as shown in *fig. 13*. Very often both types of twinning can be found in the same crystal block. (In rare cases twinning of a combination of both types is encountered, thus an intergrowth of a right-hand crystal with a left-hand crystal rotated 180°.)

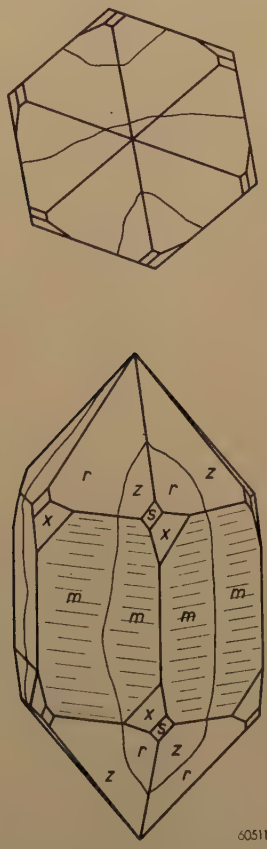

Fig. 12. Electrical twinning, drawn for a crystal with ideal faces. In well-developed crystals, such a twinning may be revealed by the presence of extra *s* and *x* faces (compare with fig. 2*a*). The irregular boundaries, drawn with thin lines, between the differently oriented crystal individuals in general are hardly if at all visible. They may be traced by the different brightness of the adjacent areas on the *r* and *z* faces and/or as sutures interrupting the horizontal striations that in general appear on the *m* faces. The only certain way to trace the twin boundaries, however, particularly if only a few or no faces are present, is to sandblast the crystal to roughen the smooth surfaces and then etch the crystal for about 10 hours in cold concentrated ammonium bifluoride solution.

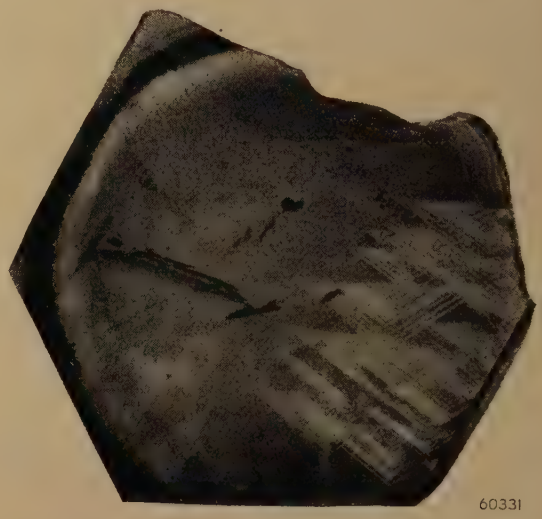

Fig. 13. Optical twinning. With this type of twinning a right-hand quartz contains more or less regularly bounded inclusions of left-hand quartz (or vice versa), which become visible on observation in polarized light. The inclusions often occur as thin regularly spaced laminae. In the photograph shown the regularity of the twin boundaries is truly remarkable.

Fig. 2, with the positive axis directions assigned by convention, represents a right-hand crystal. For a crystal of the left-hand modification the steps in cutting are exactly the same as those described above. The angles of the various low temperature coefficient cuts with the *Z*-axis are opposite for the two kinds of quartz, but the above-mentioned *r*-*z* rule still holds. When the same saw must be used for right-hand and left-hand quartz, in order to prevent confusion it is simplest to keep to the same direction of rotation in adjusting the saw table and to fasten right-hand *X*-blocks to the glass plate with the positive *X*-direction upwards and left-hand *X*-blocks with the positive *X*-direction downwards [8]).

[8]) At this place, the importance of the *r* and *z* rule and its application by means of etch light figures should again be stressed. With the formerly used method of orienting the crystal, mentioned in footnote [7]), it was evidently necessary to determine also the hand of the crystal, in addition to the positive *X*-direction. Moreover, in cases of twinning errors were often made. For example the crystal shown in fig. 12 might be oriented on the basis of the polarity determined on the edge which is a region of electrical twinning, and hence the entire crystal would be cut incorrectly. — In view of the advantages of the *r* and *z* rule, it can be stated with confidence that the simple technique of the etch light figures has been one of the conditions for a successful mass production of oscillator-plates.

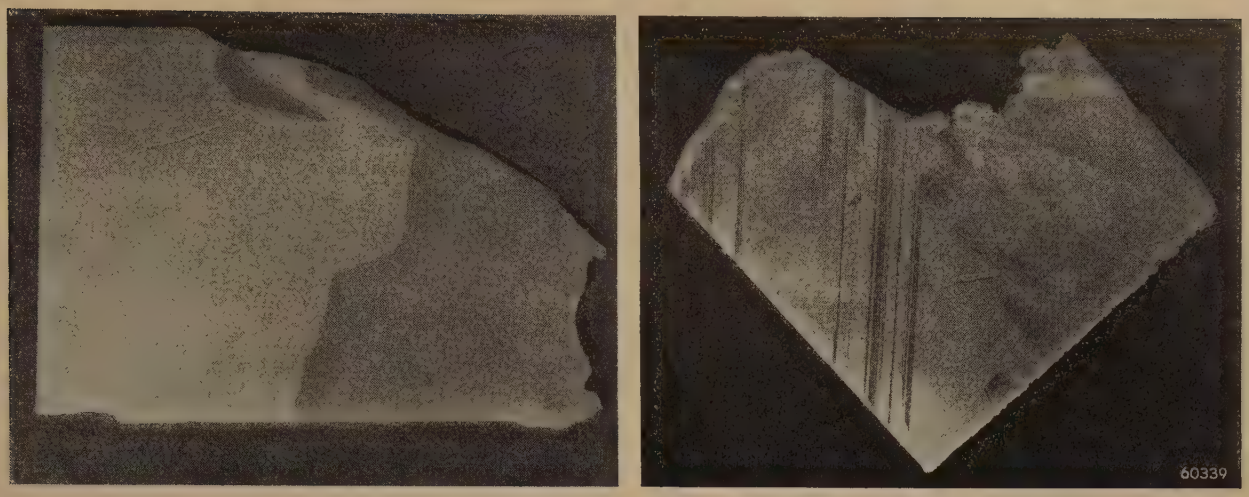

a *b*

Fig. 14. *a*) Etched wafer cut from a crystal block with electrical twinning. By means of the difference in the reflection of the two parts it is not only easy to ascertain the position of the boundary line, but also to discover which part is usable. In the case of a BT cut that part can be used which, upon being viewed at an angle of about 22° with respect to a perpendicular incident beam of light, reflects brilliantly once in a 360° revolution of the wafer in its own plane. *b*) Etched wafer cut from a crystal block with optical twinning. Due to the unfavorable position of the twin laminae no blanks can be cut from this wafer. If in cutting and mounting the quartz block we had started from a different *X*-axis, so that the twin laminae (which are always parallel to one of the *X*-axes) were perpendicular to the saw table, it would have been possible to cut some usable wafers from between the laminae.

An oscillator plate cut out of a quartz block in such a way that it consists of parts of different crystal individuals is not in general usable (unless the twin structure is limited to a fraction and/or to certain parts of the plate). This is easy to understand: the parts of a plate belonging to an electrical twin show an opposite charge upon identical deformation; those made of an optical twin show the same charge but resonate at different frequencies, since their crystallographic orientation differs (interchange of *r* and *z* in fig. 3).

Now, it must be realized that practically no crystals from the quartz mines are entirely free of twinning. In very many cases one encounters an intergrowth of many individuals. The sawing of oscillator plates thus takes on an entirely new aspect: it becomes a problem of prime importance, on the one hand, to cut out as many oscillator plates from a raw crystal block as possible without touching twin boundaries, and on the other hand to use as little sawing time as possible in cutting these plates [9]).

We can here only offer a few remarks about the means by which one attempts to attain these objects, the cutting "strategy".

Every wafer thas has been cut is etched to make the electrical or optical twinning boundaries on it visible (*fig. 14a, b*). Only one of the two orientations occurring in the wafer corresponds to the desired low temperature coefficient cut. The other orientation, represented in fig. 3 by the mirror image of the desired cut with respect to the *Z*-axis, does not correspond to any low temperature coefficient cut (at least not nearly enough to make it possible to obtain such by lapping off at an angle); the parts of the wafer having this orientation are thus worthless, and need not be sawed into blanks.

In order to avoid as much as possible loss of material by such useless parts of wafers, measures are taken before wafering. In fact it should be pointed out that in the first step of the *X*-block method chosen here as example, placing the crystal block with a prism face on the glass plate, generally a choice must be made among three prism faces, corresponding to cutting planes perpendicular to the three *X*-axes. This choice is decided by etching the whole crystal block and observing it in ordinary light.

The regions and boundaries of electrical twinning are clearly traced in this way. If possible the crystal block is laid on a prism face on which no twinning boundaries occur, since in that case the twinning boundaries will in general become visible on the *Y-Z* planes to be cut (after etching these too), and it will then be possible to decide whether the *X*-block will yield sufficient twin-free wafers in the direction of the AT cut, or will perhaps give a better yield

[9]) In addition to twinning, various kinds of inclusions and crystal defects also often occur in natural crystals, for which similar considerations hold.

in the direction of the BT cut (or other cuts), and whether some parts of the X-block cannot be used at all. A beautiful example is shown in *fig. 15*.

As in the case of optical twinning the crystal individuals of one kind are generally present in the form of thin inclusions, this type of twinning is not revealed by etching the crystal faces, but it becomes visible when the whole crystal block is viewed in polarized light (while immersed in a suitable liquid of the same refractive index as quartz to reduce reflection and refraction effects at the crystal bounraries). The twinning structure thus revealed must in a similar way serve as a guide in mounting and wafering the crystal.

It will be evident that due to the inspection at each stage of the cutting process much loss of material and much useless sawing can be avoided. This applies to the *X*-block method as well as to other cutting schemes developed for cutting raw crystals. Most of these cutting schemes have one or more disadvantages as compared to the *X*-block method, so there is no need to mention them in this short article. However, we must make an exception for the scheme called the *Z*-section, *Y*-bar method. This method, which is sketched in *fig. 16*, is ideally suited for crystals that are large (say more than about 1000 gms) and of exceptional quality. A description of the method is given in the legend of the figure.

Fig. 15. Etched *X*-block showing electrical twin boundary in middle, with boundary surface approximately perpendicular to crystal surface. If this block is cut along the twin boundary, each piece can then be wafered separately and there will be no loss of material. If wafered prior to cutting apart, then one half of each wafer will be useless (cf. fig. 14*a*).

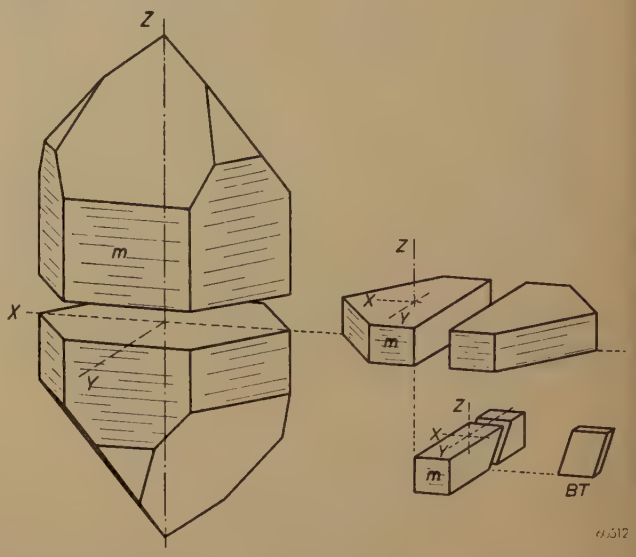

Fig. 16. In the case of large quartz crystals of exceptional quality, instead of the *X*-block method, the so-called *Z*-section *Y*-bar method can better be applied. First, sections are sawed out of the block perpendicular to the *Z*-axis, each section with a thickness about equal to the width of the desired square oscillator-plates. From the section, bars are cut whose direction of length is parallel to the *Y*-axis, and whose thickness is also equal to the width of the desired oscillator plates. A bar is now turned 90° from the position shown in the figure and mounted on the saw table. As an *X*-axis is then vertical, the bar can be turned to the correct angle and cut in the same way as an *X*-block, but instead of wafers, slices are obtained having roughly the dimensions of the final oscillator plates, and which need only be lapped and finished.

A saving in sawing time compared with other methods is realized because the sawing of blanks out of wafers is eliminated.

If there is an electrical twin boundary approximately parallel to the *Z*-axis, both parts of the *Y*-bar can be used; for the same type of cut they must be sliced at opposite angles (cf. fig. 15).

Summary. In cutting an oscillator plate out of a quartz crystal according to one of the so-called low temperature coefficient cuts, such as the AT, BT cut etc., the angle tolerances for the orientation of the crystal are very small, for example only 10 minutes. The method of obtaining the desired orientation of the crystal block under the saw is explained here, using the so-called *X*-block method for illustration. For a rough adjustment, methods based on the double refraction, amongst others, are used, while all ambiguity as to the direction of rotation of the saw table is eliminated by the observation of light patterns on etched crystal surfaces. Then the crystallographic position of a test cut is determined very accurately by means of an *X*-ray diffraction measurement and from this the required correction in the position of the saw table is deduced. The process of cutting is greatly affected by the twinning almost universally present in natural crystals. The types of twinning are briefly discussed and their influence on the "strategy" of the cutting is explained. Etching and examination at every stage of the cutting process gives greater yields and eliminates useless sawing.

PERCEPTION OF CONTRASTS WHEN THE CONTOURS OF DETAILS ARE BLURRED

by A. M. KRUITHOF.

612.843.355

The degree of contrast sensitivity is important when judging the performance of the human eye. Various investigators have made a study of contrast sensitivity in order to ascertain how far it is governed by such factors as the size and shape of the details observed and the brightness of the background. Little is known, however, about the influence that a blurring of the contours of the detail to be observed has in this respect. It is of importance to know more about this in connection with radiological, photometrical and pyrometrical investigations and for observations in the free field. To this end some experiments have been carried out whereby attention has been paid not only to the organs of the eye used in daytime (the cones) but also to those used at night (the rods).

Introduction

Visual perception is a complicated process. The eye is called upon to fulfil a great variety of tasks, whilst moreover it is expected to perform these duties with sufficient accuracy under greatly differing conditions of brightness.

One of the most important of these tasks is the perception of contrasts. In many cases it is a matter of distinguishing spots having a brightness differing but very little from that of the background against which they are seen.

Many investigators have taken measurements in respect to this perception of contrasts, whereby, inter alia, the size and shape of the spots, the brightness of the background and even the brightness of the surroundings of the actual field of observation have been varied [1]). In these investigations the measurements have mostly been confined, as far as brightness is concerned, to observations where almost exclusively the cones are used.

In some investigations the size and shape of the spot to be observed have been mainly left unchanged, only the contour being altered, for instance by giving it a saw-tooth or sinusoidal form. Little attention has been paid so far to the question as to what the influence may be of a gradual change of the brightness in the area bordering upon the spot to be observed. Yet this is a problem that is encountered in several methods of observation.

We have in mind here, in the first place, radiological examinations. In an X-ray image there is blurring due to the manner in which the image is formed [2]). Obviously this blurring affects perception when the spots to be studied are of the order of size of the blurred area. The same applies in regard to the blurring that often occurs as a result of the structure of the object (e.g. in the case of a gradually spreading pulmonary process). These two kinds of blurring may also affect the perceptibility of larger spots, and it is likely that the extent of their effect is related to the brightness of the image [3]).

This problem is also encountered in photometry. In visual photometry it is often a matter of observing the contrast between two degrees of brightness differing but little one from the other. One must then know whether, in order to get accurate results, it is necessary that the fields of different brightness are sharply defined.

In pyrometry, too, such a problem arises. In the case of the pyrometer working according to the principle of the disappearing wire, the brightness of an incandescent filament is made visually equal to that of the image of the object. For accurate measurements of low temperatures high brightness of the image is desired, and this is favourably influenced by a large aperture of the pyrometer. An objection against a large aperture is that blurring may occur along the filament [4]). The question now arises how far this affects the accuracy of the measurements.

[1]) A summary of these investigations has been given, e.g. by A. A. Kruithof and H. Zijl, Illumination intensity in offices and homes, Philips Techn. Rev. **8**, 242-248, 1946.

[2]) G. C. E. Burger, B. Combée and J. H. van der Tuuk, X-ray fluoroscopy with enlarged image, Philips Techn. Rev. **8**, 321-329, 1946; H. A. Klasens, The blurring of X-ray images, Philips Techn. Rev. **9**, 364-369, 1947.

[3]) The problem of blurring of contours is encountered also when taking observations with a radar screen.

[4]) See C. O. Fairchild and W. A. Hoover, J. Opt. Soc. Amer. **7**, 543-579, 1923.

Middleton [5]) has investigated the effect of blurred contours upon contrast sensitivity, being led thereto when considering a problem differing greatly from that just mentioned above, namely the visibility of objects in a mist. In a fog the shape of objects cannot be sharply discerned owing to phenomena of scattering along the boundaries. Middleton's measurements were taken with a field 7.5 cm × 12 cm divided into two areas with a gradual transition of brightness, and with a variable width of the blurred "edge". The brighter part of the field had a brightness of 32 cd/m² [6]). The surroundings were dark or had a brightness amounting to one-fifth of that of the actual field of vision. It was found that the contrast threshold suddenly increased when the transitional area was made so wide as to be seen at an angle of 7′ to 8′. At the brightness of 32 cd/m² (the only level at which the investigation was carried out) the organs of the eye in action are the cones.

In view of the possible fields of application mentioned above it is desired to investigate this effect more fully, it not being sufficient to confine the investigations to brightnesses where the day organs are used. It is also necessary to ascertain what happens when the rods are in use, and in particular when having regard to the application of the results to radiological observations. An X-ray image on a fluorescent screen has a brightness of 0.0003 to 0.006 cd/m², which is so low that only the elements for night sight are brought into action when one studies that image. When, however, a radiograph is made and the photographic plate or film is studied in the light of a viewing box, the brightness of the same image is so much greater that the cones of the eye are used. It is therefore of importance to investigate whether the effect of a blurred contour upon visibility is the same in both cases.

It is not likely that this blurring will have the same effect for high and for low levels of brightness, since it is common knowledge that whereas contours can quite well be sharply (accurately) observed with the organs used in daytime such is practically precluded with the organs for night sight; as everyone can easily determine for himself, at night it is very difficult to discern sharply the outlines of an object. This is accounted for by the construction of the retina of the eye. The part of the retina normally used brings far more cones into play for daytime sight than the number of rods that come into action for night sight. This is because the cones lie much closer together than the rods, whilst moreover the rods are connected in groups (with a diameter corresponding to an angle of about 20′) to one nerve fibre whereas the majority of the cones are connected to a nerve fibre of their own. As a consequence of this structure of the retina one may expect for cone sight a resolving power such that details of 0.5-1′ can still be perceived, whereas for rod sight the limit will certainly not be lower than 20′.

The effect of blurred boundaries can be studied for all levels of brightness of the background and for different dimensions and shapes of the spot. It should be possible to carry out these measurements not only with white light but also with coloured light, but it was not our intention to extend our investigations so far as that. We have confined our experiments to the case of circular spots of one certain diameter and to a high and a low level of brightness of the background, for which 50 and 0.0025 cd/m² respectively were chosen. The colour of the light was determined by the colour temperature of the incandescent lamp, viz. approx. 2800 °K.

Principle of the experiments

When we have a background with a brightness B and a spot is projected thereon in such a way that its brightness is ΔB greater (or smaller), then we call $\Delta B/B$ the contrast. If ΔB is the smallest still perceptible difference in brightness we call $B/\Delta B$ the contrast sensitivity.

If we now denote the contrast sensitivity by $B/\Delta B$ for the case where the spot is sharply defined and by $B/\Delta' B$ for the case where the spot has a blurred contour, then the ratio of the contrast sensitivity in the case of blurring to that in the case of a sharp delineation is given by $\Delta B/\Delta' B$. If the sharply defined spot can be seen better than the blurred spot then $\Delta B/\Delta' B$ is less than 1.

The experiments to be described here furnish a relation between $\Delta B/\Delta' B$ and the width of the blurred boundary zone. It is to be expected a priori that for very narrow zones $\Delta B/\Delta' B$ will be equal to 1 and for wider zones less than 1. For the lower level of brightness $\Delta B/\Delta' B$ will presumably assume values less than 1 at a greater width of the boundary zone than will be the case for the higher level of brightness, owing to the fact that at a low level of brightness the rods are used, with which we cannot see so sharply.

We shall now first describe the set-up used for these experiments for measuring $\Delta B/\Delta' B$ as a function of the boundary width.

[5]) J. Opt. Soc. Amer. **27**, 112-116, 1937.

[6]) cd = candela, the now internationally accepted denomination for the standard candle; see Philips Techn. Rev. **10**, 150-153, 1948 (No. 5).

Description of the set-up

The experimental apparatus employed is represented diagrammatically in *fig. 1*. A white screen S (30 cm × 30 cm) with a reflection coefficient of 0.80 is illuminated with an incandescent lamp (not drawn) to a brightness of 0.0025 or 50 cd/m². The surroundings of the screen are not entirely dark but have a brightness of one-fourth to one-third of that of the screen. A circular, screened, piece of frosted glass M receives light from the lamp P and is projected with the aid of a three-fold lens L onto the screen S, the dimensions being so chosen that the image has a diameter of 3.5 cm. The lamp P can be moved along rails, so that M can be given the desired brightness by varying the distance between the lamp and the glass.

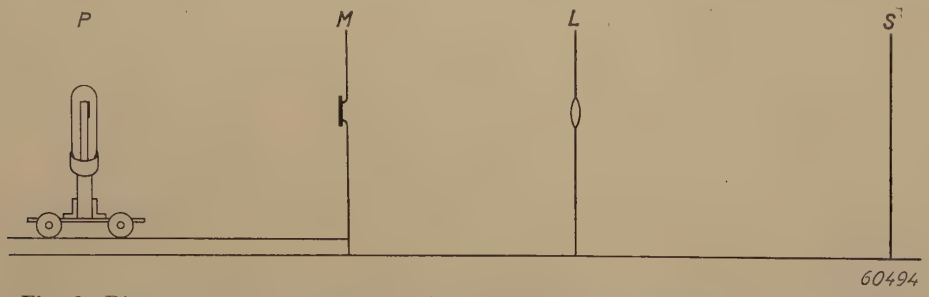

Fig. 1. Diagrammatic representation of the experimental apparatus. P the movable lamp, M the frosted glass, L the lens, which can be moved either in the direction of the frosted glass or towards the screen S.

The image of the piece of frosted glass forms on the screen a spot having a greater brightness than the background. The observer takes up a position 60 cm away from the screen and sees a spot with a diameter of 3.5 cm viewed from an angle of 3.5 °. Of course it depends upon the difference in brightness between the spot and the screen whether he does indeed see the image or not.

Let us suppose that the distances are so chosen that the lens casts a sharp image of the frosted glass on the screen. Upon the lens being moved, either in the direction of the screen or in that of the frosted glass, the image on the screen will be blurred, and the greater the displacement of the lens the wider will be the area of confusion.

When, after focusing, the lens is moved towards the screen the passage of the rays will be as indicated in *fig. 2*. From the similarity of triangles it follows that $p - q = (d/b) \cdot 2r$, where $p - q$ denotes the width of the area of confusion, d the distance of the screen behind the image plane, b the image distance and $2r$ the diameter of the lens. For the case where the lens is moved towards the frosted glass we find in the same way $q - p = (d/b) \cdot 2r$, where d is then the distance of the screen in front of the image plane.

The distance between the frosted glass and the screen is kept unchanged. From this distance, the focal length of the lens, the diameter of the lens, the object distance ML and one of the above formulae one can then calculate the width of the area of confusion in mm. From this width one can calculate the visual angle from which the observer sees the area of confusion, since the distance between the observer and the screen is known. In *table I* the lens displacements are given which were needed in our experiments to get an area of confusion of a certain width (expressed in arc units).

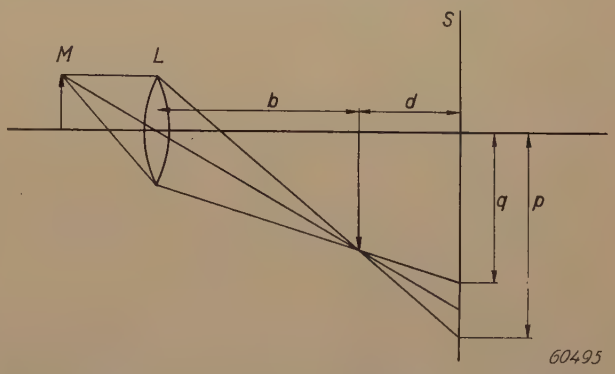

Fig. 2. Passage of the rays in the formation of an image with an area of confusion. M the frosted glass, L the lens, S the screen, p—q the width of the area of confusion, b the image distance and d the distance of the screen behind the image plane.

Table I. The lens displacements which were necessary to get an area of confusion of a certain width (expressed in arc units) and the extra brightness ΔB of the central part of the spot on the screen with a brightness $B = 50$ cd/m² at these distances from the lens.

Width of area of confusion (in ′)	Lens displacement in the direction of S (in mm)	Lens displacement in the direction of M (in mm)	Extra brightness ΔB (in cd/m²) of the central part of the spot when shifting the lens in the direction of	
			S	M
0.0	—	—	2.92	2.92
2.4	2.7	2.3	2.93	2.88
6.0	6.8	5.0	3.01	2.84
12	14.1	10.0	3.07	2.77
24	29.2	19.0	3.22	2.67
36	60.0	27.0	3.54	2.63

The variation of the brightness in the area of confusion is of a simple nature if it is permitted to assume that the frosted glass and the screen have a distribution of radiation according to Lambert's law at least for directions making a small angle with the normal, and if, moreover, the distances from M to L and from L to S are great with respect to the diameters of M, L, the spot and its area of confusion. To get an idea of this variation of the brightness, let us take a look at *fig. 3*, where PQ represents the width of the said area.

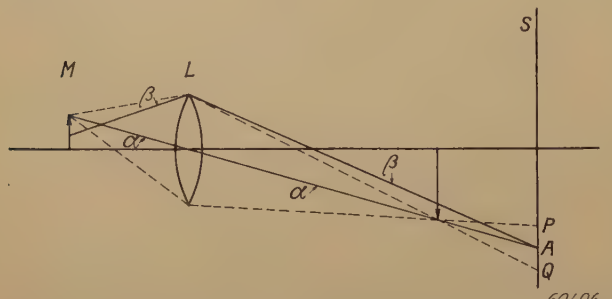

Fig. 3. Diagram illustrating the change of brightness in the area of confusion PQ. α and β are the boundary rays of the beam determining the brightness at A.

Above P one observes the full brightness of the spot, and below Q the brightness is zero. Halfway between P and Q is the point A where the rays merge that are contained in the beam bounded by the rays α and β. In the same way one can draw in the cross section under consideration for any point of the spot and its boundary zone the marginal rays of the beam producing the brightness at that point.

By carrying out the following experiment in our imagination we can form a picture of the cross section of the conical beam reaching the screen at any arbitrary point A' between P and Q. We put our eye at a point on the screen above P and direct it upon the image of the frosted glass formed by the lens, which it is assumed could be perceived in the image plane. If this "image of the frosted glass" were made visible we should see it as a very large circle. Our eye, placed at a point of the screen above P, sees the lens as a small circle lying entirely within the "image of the frosted glass". Now we move our eye in the direction towards P and then via A' to Q. The small circle (the lens) will then first approach the boundary of the large circle (the image of the frosted glass), which is practically a straight line, and then cross it. This is schematically represented in *fig. 4*. The lens is only visible in its entirety so long as the cone with the eye as apex passing through the circumference of the lens falls within the cone having the same apex and passing through the circumference of the image of the frosted glass. When we reach with our eye a point on the screen where the first cone falls only partly within the second one, that point will receive less light. When the eye has reached Q the lens circle crosses the boundary of the image of the frosted glass; one cone then lies outside the other, and at this point the frosted glass no longer gives any brightness.

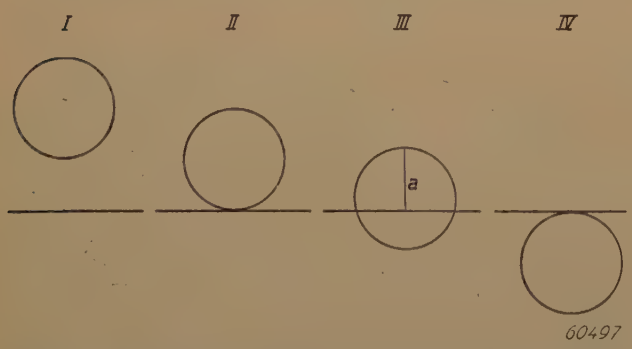

Fig. 4. Position of the image of the lens with respect to the "image of the frosted glass" in an imaginary experiment where the eye is moved to different points of the screen. The horizontal line represents the edge of the (very large) image of the frosted glass and the circles represent the image of the lens. The four illustrations relate to the cases where the eye is situated: I above P (see fig. 3), II at P, III at a point A' between P and Q, and IV at Q.

If this can be understood then it is clear how the brightness of the points between P and Q can be calculated. This brightness is proportional to the area of the segment of the lens circle observed in the points of this zone above the edge of the image of the frosted glass. A segment with the height a (fig. 4) corresponds to a point A' at such a distance between P and Q that $QA' : A'P = a : (2\varrho - a)$, where ϱ is the radius of the image of the lens.

The calculation shows that the brightness in the area of confusion varies approximately in a straight line. It is found that the distribution of brightness of the spot with its area of confusion is as represented diagrammatically in *fig. 5*. To a first approximation this figure is a trapezium. From the description of the set-up of the apparatus depicted in fig. 1 it follows immediately that the brightness of the central part of the spot undergoes a change when the lens is displaced either in one direction or in the other. Thus the height of the trapezium in fig. 5 depends upon the position of the lens. Consequently, when measurements are taken after the lens has been displaced, a correction has to be made.

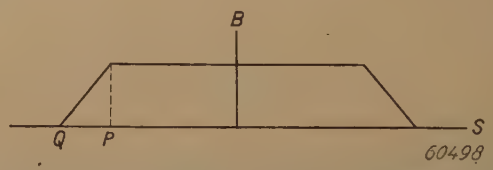

Fig. 5. Diagram showing the change of brightness B in the spot and in the area of confusion. P and Q relate to the points denoted by these letters in fig. 3.

With a view to making this correction the brightness of the central part of the spot was determined for the various positions of the lens before lighting the lamp illuminating the whole of the screen. With the lamp P at a certain distance from the frosted

glass M the illumination in the spot on the screen S was measured with the aid of a selenium cell, and from that the brightness was calculated. This was repeated after the lens (with P at the same distance) had been shifted to one of the positions given in table I. The increase of the brightness of the spot in cd/m² with the respect to the brightness of 50 cd/m² of the screen is also shown in table I. The position of the lens is characterized by the angle at which the observer sees the boundary zone of the spot with the lens in the respective position [7]).

For the lower brightness level of the screen (0.0025 cd/m²) the brightness of the spot was reduced to the desired level with the aid of neutral filters of a known transmission.

How the measurements were taken

In carrying out these measurements two people worked together, one of whom will be called the observer and the other the investigator.

The observer is the one who took up a position 60 cm away from the screen and during the experiments adjusted the contrast so that he could just perceive the spot; he does this by placing the lamp P in such a position that he sees the spot appear in the background or disappear.

For our experiments we had two male observers, one 26 and the other 35 years of age, whose eyes showed no particular aberrations and whose contrast sensitivity may be taken as normal.

The investigator noted the position of the lamp after each adjustment, without communicating this to the observer.

A series of experiments begins with the observing of a spot that is sharply delineated. Then by gradually increasing the distance between the lamp and the frosted glass the observer makes 10 adjustments in succession until he can just no longer see the spot, after which he makes 10 more adjustments by drawing the lamp towards the frosted glass until the spot just becomes visible. The arithmetical mean of the 20 brightnesses of the spot corresponding to these adjustments gives the contrast sensitivity of the observer with the given brightness of the background and a sharply delineated spot seen at an angle of 3.5 degrees.

Next, the lens is moved, for instance first towards the screen, over such a distance that the spot has an area of confusion of 2.4′, at which distance the 20 measurements are taken again. These are repeated once more after the lens has been moved in the opposite direction so far that the spot again has an area of confusion of the same width. After a correction has been made for the changed brightness of the spot as indicated in table I, these 40 measurements give the contrast sensitivity of the same observer for the same brightness of the background and a spot of 3.5° diameter with an area of confusion of 2.4′.

The contrast sensitivity for the other widths of the area of confusion given in table I is determined in the same way. It is then possible to calculate the ratio $\Delta B/\Delta' B$ as function of the width of the area of confusion.

Care has to be taken that the part of the spot with the maximum brightness always has a diameter of approximately 3.5 degrees, this being done by adjusting the diaphragm in front of the frosted glass.

It was found impracticable to carry out all these adjustments after the other because it was too tiring for the observer. When a series had to be interrupted it was resumed next day by starting again with observations of the sharply delineated spot and then carrying on with the remaining observations of the spot with blurred edge.

It has to be added that when the adjustments were made the observer had to rest his head in a certain way against a support, so that both the distance from the screen and the position of the head were fixed.

In these experiments one has to rely upon the observer's promise not to fix his eye outside the spot. Fixing of the eyes upon the right place is particularly necessary when the experiments are carried out at the very low brightness of 0.0025 cd/m². At such a low level there is a natural tendency not to fix the eye on the spot, because the sensitivity of the eye outside the central part of the retina is then greater than the sensitivity in that part itself, whilst with higher levels of brightness the reverse is the case. It goes without saying that the room in which the experiments were conducted was otherwise quite dark, and that the observer was given ample time (about 15 minutes) to adapt his eyes to the brightness of the screen and his surroundings.

Results of the experiments

Extensive experiments with the aid of the apparatus described and two observers each completing the full series of adjustments with a background brightness of 50 cd/m² yielded the results tabulated in *table II* and graphically represented in *fig. 6*.

[7]) The changes in brightness can also be found by calculation. The corrections determined in this way were in agreement with the results of the measurements.

Table II. Change of the contrast sensitivity of two observers as function of the width of the area of confusion of a spot against a background brightness of 50 cd/cm².

Width of area of confusion (in ′)	$\frac{\Delta B}{\Delta' B}$ first series	$\frac{\Delta B}{\Delta' B}$ second series	$\frac{\Delta B}{\Delta' B}$ average
0	1.00	1.00	1.00
2.4	1.055	1.02	1.04
6.0	0.99	1.03	1.01
8.4	—	0.86	0.86
12	0.69	0.77	0.73
24	0.585	0.775	0.68
36	0.625	0.715	0.67

It appears that up to a width of about 7′ for the area of confusion there is no decline in the contrast sensitivity, but that it then diminishes rapidly to about two-thirds of the original value until a width of 12′ is reached, after which it remains practically constant.

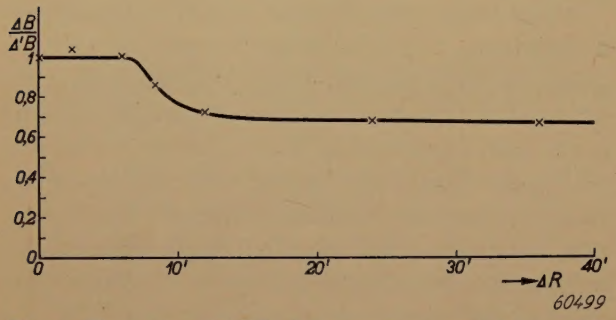

Fig. 6. The ratio $\Delta B/\Delta' B$ of the contrast sensitivities when observing a sharply delineated spot and a spot with an area of confusion, as function of the width of that zone against a screen brightness of 50 cd/m². The width of the area of confusion ΔR has been plotted along the horizontal axis. Each point of the curve is the result of 160 adjustments.

The width of the blurred edge where contrast sensitivity begins to diminish according to our experiments is the same as that which Middleton found in his investigations mentioned above. His measurements too give an indication that with greater widths of the area of confusion there is a less pronounced decline in contrast sensitivity, but there was not such a marked return to a practically constant value, and the width of the area of confusion where this began was greater. This may be due to the fact that Middleton used a test object of larger dimensions and different shape. We are of opinion, however, that the decline found from both investigations at 7′ to 8′ is connected with the nature of the retina, having regard to the distance between the cones and the nerve connections at and possibly between the cones.

The experiments described above were also carried out with the two observers when the screen had a lower level of brightness (0.0025 cd/m²).

Table III. Change of contrast sensitivity (average of two observers) as function of the width of the area of confusion of a spot against a background brightness of 0.0025 cd/m².

Width of the area of confusion (in ′)	$\frac{\Delta B}{\Delta' B}$
0	1.00
2.4	1.08
6.0	0.95
12	0.97
17	0.97
20.5	1.08
24	0.82
36	0.83

The average of the results of their observations is given in *table III* and represented in *fig.* 7.

It appears that with this background brightness the ratio of the contrast sensitivity for sharp delineation and for a blurred contour is constant until an area of confusion of about 20′ is reached, after which it drops rather suddenly to about 0.82. Since the angle of 20′ also plays a part in the structure of the retina there is reason to assume that the cause of the reduced contrast sensitivity at this width of the area of confusion is connected with the composition of the rod system.

It is seen that both when the cones are used and when the rods are brought into action there is a decline in contrast sensitivity as soon as the area of confusion exceeds a certain width. Under otherwise the same conditions the reduction when the rods are in action is less than that when the cones are used, but then it must of course be borne in mind that when the organs of day sight are in use contrast sensitivity is very much greater (25 to 50 times) than when the organs of night sight are used.

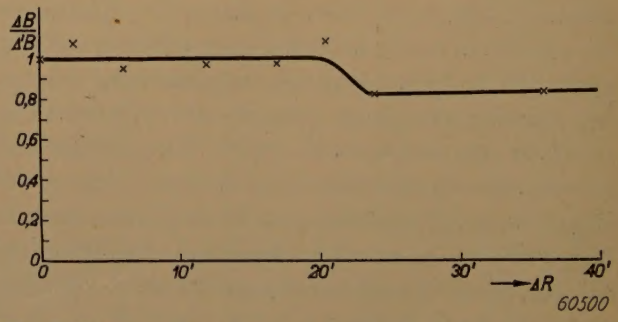

Fig. 7. The same function as plotted in fig. 6, but for a screen brightness of 0.0025 cd/m². Each point in the curve is the result of 80 adjustments.

Some conclusions

From the experiments described here it follows that in radiological examinations, both with high and with low brightness levels, blurred contours of the image will only slightly affect visibility, at

least where it is a matter of observing contrasts in relatively large objects.

It appears that in photometry a sharply defined boundary is not strictly necessary. If a photometer is so constructed that the transition between two areas of almost the same brightness is gradual this need not prevent accurate results being obtained.

In the case of optical pyrometers the effect observed means that larger apertures can be used, and thus lower temperatures measured, without any noticeable loss of accuracy.

Summary. The observing of contrast is an important duty of the eye. In most cases it is a matter of perceiving spots differing only slightly in brightness from the background against which they are seen. In connection with various applications (radiological examinations, photometry, pyrometry) it is of importance to investigate experimentally in how far blurring of the contours of a spot that is to be observed affects the contrast sensitivity of the eye. A description is given of the apparatus used for such an investigation. Experiments have been carried out with a round spot (diameter 3.5 cm) projected in such a way that its brightness was slightly greater than the background; two cases were taken, viz. with screen brightnesses of 50 and 0.0025 cd/m². It appeared that when the daytime organs of sight are used (the cones) contrast sensitivity is not reduced by a blurred contour until the width of the area of confusion has grown to an angle of about 7′, when it rapidly declines to about two-thirds of its original value at an area of confusion having a width of 12′, after which it remains practically constant. When the organs of night sight are used (the rods) there is a slight decline in contrast sensitivity when the width of the area of confusion is extended to about 12′. From these results some conclusions are drawn for the above-mentioned technical applications.

ABSTRACTS OF RECENT SCIENTIFIC PUBLICATIONS OF THE N.V. PHILIPS' GLOEILAMPENFABRIEKEN

Reprints of these papers not marked with an asterisk can be obtained free of charge upon application to the Administration of the Research Laboratory, Kastanjelaan, Eindhoven, Netherlands.

1880: J. ter Berg and G. J. van Wijnen: The porosity of welds (Welding J. **28**, 269 S-271 S, 1949, No. 6).

A study of external porosity in welds, as caused by sulphur. By relatively slight alterations in the composition of the coating it is possible to obtain welds free from this porosity, even with a considerable sulphur content of core wire and coating. Two methods were applied:

1) The coating was made more basic in order to absorb more S in the slag.

2) The oxidizing power of the coating was increased in order to get rid of sulphur in the form of SO_2.

1881: N. W. Smit and F. A. Kröger: The luminescence of zinc sulfide activated by lead (J. Opt. Soc. Amer. **39**, 661-663, 1949, No. 8).

Zinc sulfide activated by lead shows fluorescence in various bands, two of which can be attributed to lead. The first band has a maximum at 4850 Å, the second one at 6100 Å. The orange band is favoured by sulfurizing conditions and appears irrespective of whether halide ions are present or not. This band is attributed to a characteristic electronic transition in divalent lead ions, occupying normal lattice sites. The green band is favoured by reducing conditions and only appears when chlorine ions are present. This band is attributed to electron transfer transitions between positive and negative ions of configurations formed by monovalent lead and chlorine ions. situated at normal lattice sites, together with the neighbouring lattice ions. A green band appearing in reduced zinc sulfide is attributed to a stoichiometric excess of zinc.

1882: R. van der Veen: Induction phenomena in photosynthesis, I (Physiologia Plantarum **2**, 217-234, 1949).

Adaptation phenomena, which occur in photosynthesis when leaves are suddenly illuminated, in an atmosphere containing CO_2 can be divided into an initial sudden CO_2-uptake (I.U.), followed by a light adaptation period with constant negative slope of CO_2-content (L.A.S.). The I.U. is independent of temperature and of the length of the preceding dark period, while the L.A.S. is strongly influenced by these factors.

When leaves are exposed to a high temperature ($\pm$ 48 °C) for a few minutes and afterwards examined at normal temperature, the capacity of CO_2 assimilation is irreparably damaged, but the I.U. still exists. When the illumination is stopped the amount of absorbed CO_2 is released by such leaves.

At low temperature CO_2 assimilation is also inhibited, but the I.U. is still quite strong. At the end of the illumination the absorbed CO_2 is not released, but after a short period of darkness (less than 15 minutes) the I.U. is not maximal. The duration of the I.U. is about 20 seconds.

So in normal leaves at low temperature the I.U. is not reversible, while in heat-treated leaves it is made reversible.

In the discussion a theoretical scheme is developed to explain these facts.

1883: J. A. Haringx: Elastic stability of flat spiral springs (Appl. sci. Res. The Hague **A2**, 9-30, 1949, No. 1).

This paper deals with the elastic stability of the flat spiral spring, that is a structure consisting of a wire coiled into a spiral lying in a plane. A rough calculation, valid for spiral springs having a large number of coils, shows that the critical number of turns which the spring has to be wound or unwound to reach the state of instability is determined only by the ratio of the sides of the rectangular wire section. It depends neither upon the number of coils nor upon Young's modulus of the wire material.

In order to verify in how far this holds for a spring with a small number of coils a second and more accurate calculation is given, though only for a (fictitious) spiral spring having circular and identical coils. Further, it is shown that the realization of a spiral spring able to undergo more than, say, three turns without becoming unstable is impossible.

R 116: G. Diemer and K. S. Knol: Measurements on total-emission conductance at 35-cm and 15-cm wavelength (Philips Res. Rep. **4**, 321-333, 1949, No. 5).

For the contents of this article see these abstracts, No. **1870***.

R 117: L. J. Dijkstra and J. L. Snoek: On the propagation of large Barkhausen discontinuities in Ni-Fe alloys (Philips Res. Rep. **4**, 334-356, 1949, No. 5).

The propagation of the Bloch boundary between two macrodomains under the influence of an external magnetic field H has been investigated for Ni-Fe wires, of the composition 60-40 and 50-50, subjected to a tensile stress. The interesting quantities involved are the effective length λ of the discontinuity and the rate of propagation v. The length λ is proportional to the diameter of the wire and independent of the temperature and the working conditions. In thick, well annealed wires, at low temperature, the velocity v is determined chiefly by the counteracting field of the eddy currents. With thin wires and at high temperatures, especially in cold-worked material, another limiting factor comes to the fore, which, however, is as yet not sufficiently understood.

R 118: J. L. H. Jonker: The computation of electrode systems in which the grids are lined up (Philips Res. Rep. **4**, 357-365, 1949, No. 5).

Formulae are developed describing the path of the electrons and the position of the focus in a system of electrodes in which the grids are lined up. These are then applied to the calculation of a plane arrangement such as to possess prescribed characteristics and to have zero screen-grid current when the control grid is at zero potential.

R 119: B. D. H. Tellegen: Complementary note on the synthesis of passive, resistanceless four-poles (Philips Res. Rep. **4**, 366-369, 1949, No. 5).

By the removal of a pole at a finite value of the frequency a passive, resistanceless four-pole of order n may be split up into a second-order four-pole of order $n-2$ (see also **R 89**).

R 120: J. D. Fast: An apparatus for preparing small samples of pure iron to which fixed quantities of impurities can be added (Philips Res. Rep. **4**, 370-374, 1949, No. 5).

A high-frequency melting apparatus is described for preparing alloys of well-defined compositions in quantities up to 2000 grams (see Philips Techn. Rev. **11**, 244-247, 1949, No. 8).

R 121: J. A. Haringx: On highly compressible helical springs and rubber rods, and their application for vibration-free mountings, V (Philips Res. Rep. **4**, 375-400, 1949, No. 5).

This paper deals with the behaviour in space of the different types of vibration-free mounting, starting from the simple construction of a resiliently supported body up to the damped dynamic vibration absorber provided with an auxiliary mass. In order to simplify the problems of forced and free vibrations it is aimed at splitting up the movements in space into a number of one- and two-dimensional movements to be treated independently. In this connection it appears to be necessary to confine the present considerations to constructions where the spring and damping systems show some special properties with regard to their so-called principal axes, of elasticity and of damping. These systems of principal axes, which exist in each two-dimensional case, only exceptionally occur in space. The respective requirements can best be met by introducing in the construction a certain degree of symmetry, as is elucidated for the two- and the three-dimensional case separately. (See these abstracts, Nos. **R 94, R 101, R 109,** and **R 113.**)